Renewable Energy 163 (2021) 755–771

Contents lists available at ScienceDirect

Renewable Energy

journal homepage: www.elsevier.com/locate/renene

Improved ECMWF forecasts of direct normal irradiance: A tool for better operational strategies in concentrating solar power plants

Francis M. Lopes [a, b, *], Ricardo Conceição [a, b, c], Hugo G. Silva [a, d], Rui Salgado [a, d], Manuel Collares-Pereira [a, b]

[a] Institute of Earth Sciences, University of Évora, Rua Romão Ramalho 59, 7000-671, Évora, Portugal
[b] Renewable Energies Chair, University of Évora, IIFA, Casa Cordovil, Rua D. Augusto Eduardo Nunes 7, 7002-651, Évora, Portugal
[c] High Temperature Processes Unit, IMDEA Energy, Avda. Ramón de la Sagra 3, 28935, Móstoles, Madrid, Spain
[d] Department of Physics, School of Sciences and Technology, University of Évora, Rua Romão Ramalho 59, 7000-671, Évora, Portugal

ARTICLE INFO

Article history:
Received 3 April 2020
Received in revised form
3 August 2020
Accepted 26 August 2020
Available online 4 September 2020

Keywords:
ECMWF
Direct normal irradiance
Short-term forecasting
Model output statistics
Concentrating solar power operation
Energy production simulations

ABSTRACT

To contribute for improved operational strategies of concentrating solar power plants with accurate forecasts of direct normal irradiance, this work describes the use of several post-processing methods on numerical weather prediction. Focus is given to a multivariate regression model that uses measured irradiance values from previous hours to improve next-hour predictions, which can be used to refine daily strategies based on day-ahead predictions. Short-term forecasts provided by the Integrated Forecasting System, the global model from the European Centre for Medium-Range Weather Forecasts (ECMWF), are used together with measurements in southern Portugal. As a nowcasting tool, the proposed regression model significantly improves hourly predictions with a skill score of ≈0.84 (i.e. an increase of ≈27.29% towards the original hourly forecasts). Using previous-day measured availability to improve next-day forecasts, the model shows a skill score of ≈0.78 (i.e. an increase of ≈6% towards the original forecasts), being further improved if larger sets of data are used. Through a power plant simulator (i.e. the System Advisor Model), a preliminary economic analysis shows that using improved hourly predictions of electrical energy allows to enhance a power plant's profit in ≈0.44 M€/year, as compared with the original forecasts. Operational strategies are proposed accordingly.

1. Introduction

Numerical weather prediction (NWP) models have been improved continuously over the last decades due to advances in computational technology, meteorological analysis, physical parameterizations and numerical methods. Particularly, in the field of solar radiation forecasting, remarkable progress has been made in recent years with the constant upgrades regarding radiative and aerosol schemes implemented in NWP models. Such advances allowed NWP to provide the best possible forecasts for the two most important solar components used for solar energy harvesting, namely global horizontal and direct normal irradiances (GHI and DNI, respectively). These two solar resources are described in detail throughout literature, such as in Refs. [1].

A precise prediction of DNI is essential for the energy management of concentrating solar power (CSP) systems, particularly during partly cloudy conditions [2], in which CSP plants experience significant periods of solar intermittency. During such periods, clouds passing over the solar field lead to an energy reduction, since energy is suddenly not being collected and, at the same time, there is energy being consumed by the plant due to its operation, such as the production of electricity. Energy is mainly needed to feed the power block, but also for auxiliary consumption, such as maintaining the heat transfer fluid above a certain temperature (critical for molten salt systems). The duration of these energy deficiency periods can go from a few minutes to an entire day, depending on various atmospheric parameters such as size and depth of clouds, wind velocity and direction, and aerosols (concentration and type). The latter, while less frequent, can also significantly affect CSP energy production, as during desert dust storms [3] or severe air

* Corresponding author. Institute of Earth Sciences, University of Évora, Rua Romão Ramalho 59, 7000-671, Évora, Portugal.
E-mail addresses: fmlopes@uevora.pt (F.M. Lopes), rfc@uevora.pt (R. Conceição), rsal@uevora.pt (H.G. Silva), hgsilva@uevora.pt (R. Salgado), collarespereira@uevora.pt (M. Collares-Pereira).

https://doi.org/10.1016/j.renene.2020.08.140
0960-1481/

pollution events [4].

Although NWP models currently provide satisfactory solar radiation forecasts, depending on the forecast horizon, these have always an associated error (i.e. a forecast uncertainty). This uncertainty is a consequence of errors in the initial conditions and in the formulation of the models itself [5]. Since models provide deterministic values associated with systematic errors, the combined use of NWP data, statistical, and machine learning methods (e.g. Ref. [6]), allows the assessment of the uncertainty associated with the forecast results. The statistical post-processing of dynamical NWP outputs can be of practical use for weather forecasting [7], in which two main categories of classification for statistical downscaling methods exist [8]: perfect prognosis and model output statistics (MOS). Perfect prognosis [9] consists in the development of statistical relationships between large-scale free atmospheric and local surface variables (both sets of data are originated from historical or actual observations). Whereas in MOS [10], the free atmospheric variables are originated from numerical model outputs. Each method has its own advantages and disadvantages, but, essentially, MOS accounts for systematic model errors (e.g. dry bias) with the use of multiple predictors, allowing for a better fit to the predictand data and higher accuracy. Such accuracy, is generally better than pure statistical models, which have a high performance at very short time resolutions (<30 min) within the nowcasting range (i.e. from 0 to 6 h), or pure NWP models, which go beyond the 6-h range. After combining observations with NWP model outputs, statistical techniques, such as the use of statistical regression models (the most basic form of MOS), can be applied to derive forecast equations, allowing to improve the original forecasts [11]. To reduce NWP uncertainty and improve the systematic error correction of DNI forecasts, several statistical methods have been used. In Ref. [12], a simple post-processing correction was implemented over 3-h average values of predicted DNI, leading to satisfactory results with correlations in the order of 0.9. In their work, the authors concluded that clouds were the main source of numerical bias. In Ref. [13], a third-degree polynomial fit was performed over monthly mean hourly values, providing a high correlation coefficient of about 0.96 between the clearness index and historical DNI data. Depending on the forecast horizon, several other more complex approaches have been used to evaluate the systematic errors. For instance: Multi-Model [14]; Multi-Parameterization [15]; Stochastic Parameterization [16]; Multi-Parameter [17]; Stochastic Kinetic Energy Backscatter methods [18]; artificial neural networks [19]; autoregressive integrated moving average (ARIMA) models [20,21]; assemble MOS [22], among others. Besides statistical downscaling methods, the nesting of high-resolution limited-area models in global models (i.e. dynamic downscaling) can also be used to improve NWP outputs. As described by Ref. [23], the method has the advantage of not requiring local observations and the potential to provide better results than statistical methods, particularly the prediction of extreme events. However, the throwback lies in the fact that systematic errors present in the global models are propagated to the mesoscale ones. Moreover, higher computational cost is needed for implementing a high-resolution model.

In addition to NWP uncertainty, there are also particular difficulties in providing accurate forecasts of DNI due to the inaccurate prediction of clouds and aerosol concentrations. The misrepresentations of clouds and aerosols in the atmosphere significantly reduce the accuracy of the forecasted DNI, as these are the two main modulators of solar radiation at the surface [12]. For instance, extreme aerosol effects such as desert dusts, which are known to reduce the DNI up to 90% [24], are generally misrepresented in the models. Although aerosol implementation in NWP is commonly considered in several operational forecast models, the actual concentration levels are not predicted. Thus, its total effects in the radiative forcing mechanism (and therefore in solar radiation at the surface) are still not accurately represented [25]. Currently, the majority of NWP models consider monthly mean aerosol climatologies, not allowing to represent the actual aerosol content in the atmosphere, particularly on the hourly and daily resolutions. Moreover, despite the fact that cloud formation processes are quite well understood, the representation of clouds in NWP models is the most significant factor that contributes to the lack in DNI accuracy. This occurs not only during overcast periods, but also, and more severely, under partly cloudy days due to the complex nature and scale of cloud microphysical mechanisms. At such small scales, nonlinear and turbulent motions contribute to a chaotic and stochastic system, as oppose to deterministic [26]. For instance, during partly cloudy days, models are roughly able to predict that clouds will appear, however the exact location and timing of cloud formation and dissipation (i.e. cloud life cycle) are difficult to predict. This occurs especially for mesoscale clouds, i.e. below a horizontal resolution of several kilometres.

In this work, state-of-the-art statistical downscale methods are presented for the correction of the systematic error associated with hourly predictions of DNI to improve CSP plants operational strategies, an important information for the plant operator. In this context, day-ahead forecasts (i.e. next 24-h) of DNI from the Integrated Forecasting System (IFS), the global NWP model from the European Centre for Medium-Range Weather Forecasts (ECMWF), are used together with local measurements considering a period of two years in Évora (southern Portugal). The novelty of this work is based on the use of improved hourly and daily predictions from the ecRad (cycle 43R3) radiative scheme of the IFS to establish generic next-hour and next-day CSP operational strategies. To this end, several regression models are created, where a compound multivariate regression model (designated here by MRM2) that uses previous measured hour of irradiance values to forecast next-hour values (i.e. within the nowcasting range) is proposed. In order to define generic daily operational strategies, the proposed methodology combines improved daily availabilities of DNI (also important for day-ahead energy dispatchability operations) with improved hourly predictions to refine hour-by-hour operational procedures that occur throughout the day. Moreover, hourly predictions are used in the System Advisor Model (SAM), from the National Renewable Energy Laboratory (NREL), to simulated electrical energy values from a CSP plant with similar configurations to the Andasol 3, i.e. a conventional linear focus parabolic-trough system. The resulting electrical energy outputs of the simulated CSP plant based on measured, predicted and improved predicted data, are then analysed and compared as a rough verification of the implications of the DNI forecast improvement.

It should be noted that the present methodology is not limited to one region only, since it can be performed in other regions of high solar potential, such as in arid climates, ideally, far from major sources of pollution (e.g. southern Spain, northern and southern Africa, south and north America, northern Australia, and Saudi Arabia). Applying the proposed procedures of this work in other regions of interest, in which accurate DNI forecasts are demanded, will improve the regional management and, consequently, energy efficiency of solar electrical power plants.

After the introductory section, the remainder of the present paper is structured as follows: measurements, forecast model and power plant model are described in Section 2; the considered methodology is presented in Section 3, including evaluation metrics and applied statistical methods used; results are given in Section 4; the use of improved forecasts for CSP operations is discussed in Section 5; conclusions and future perspectives are briefly outlined in Section 6.

2. Data

2.1. Measurements

A ground measuring station (designated here by EVO station) located in southern Portugal, namely in Évora city (38.567686°N, 7.911722°W), was used to perform 1-min recordings of solar radiation. Measurements were carried out during a period of two consecutive years, i.e. from July 1st 2017 to June 30th 2018 and from July 1st 2018 to June 30th 2019. The selected location stands as a semi-arid region (cf. [27]), characterized by clean atmospheric conditions with high DNI annual availability values and low variability [28]. The optimal conditions for solar harvesting allowed the installation of several already operational solar power stations in the region, with more solar projects being foreseen to take place.

Continuous measurements were performed using state-of-the-art instrumentation. A pyranometer (model CMP11) was used to measure GHI, according to the International Organization for Standardization (ISO) 9060 Secondary Standard [29], with an associated estimated uncertainty (i.e. estimates of observation error) below 2% on a daily basis. In the case of measured DNI, a pyrheliometer (model CHP1) was used, according to the ISO 9059:1990 standard [30], with an associated estimated uncertainty below 1% on a daily basis. Both instruments were mounted on a SOLYS2 Sun-Tracker (Kipp & Zonen) installed at the Institute of Earth Sciences (ICT - *Instituto de Ciências da Terra*) observatory in the University of Évora. The solar measuring equipment has been operational since 2015, with a daily basis cleaning protocol in order to prevent any anomalous recordings due to equipment malfunction (e.g. sudden power shutdowns) or soiling deposition [31].

For the same period of study, standard meteorological equipment was used to measure EVO meteorological data, including air temperature and relative humidity through the use of a hygrothermo transmitter model 1.1005.50.512 (Thies Clima), installed near the SOLYS2 Sun-Tracker. Additionally, wind velocity and surface air pressure at 10 m height were also recorded using an anemometer model A100R (Vector Instruments) and a barometric pressure sensor model PTB101B-CS105 (Campbell Scientific), respectively. It should be noted that, in EVO station, surface pressure is not available, and the wind is not representative, since the flow is disturbed by nearby buildings. For these reasons, hourly data from the Portuguese meteorological service station (IPMA – *Instituto Português do Mar e da Atmosfera*), located at Évora aerodrome (38.53654N, 7.88795W), i.e. about 4 km apart from EVO station, was used as representative of the wind velocity and surface pressure in EVO.

Together with DNI measurements, this set of meteorological data is required as input for the simulation of a linear focus parabolic-trough system to assess the resulting CSP plant performance outputs, as shown in Section 5.

After acquiring all the measured data needed, prior to the analysis, data quality control procedures were carried out, as described in Section 1 (Appendix A). After the application of the proposed filters, and in order to compare with the predicted data, measured hourly values were calculated through hourly backward means, i.e. by considering the previous sixty 1-min records of measured data.

2.2. Forecast model

To simulate atmospheric processes, NWP models make use of equations based (as much as possible) in the fundamental principles of physics, requiring large computational effort. Among a wide range of current operational models, the IFS, the global model from the ECMWF, stands as one of the highest scored NWP models in terms of medium range global weather forecasting capacity [32]. The radiative scheme currently used in the IFS, the ecRad (cycle 43R3), provides hourly forecasts of DNI and GHI, among a wide range of available parameters. In order for the model to produce solar radiation outputs, several prognostic variables, such as temperature and cloud fraction, are interpolated horizontally into the radiation grid through cubic interpolation on an hourly basis [33]. Moreover, the IFS uses the Copernicus Atmosphere Monitoring Service (CAMS) system [34], an improvement towards the previous versions implemented in the model, for instance Ref. [35], providing the aerosol climatology.

In this work, day-ahead forecasts (i.e. next 24-h) from the IFS are used for a post-processing analysis considering local measurements over a grid of $0.125° \times 0.125°$. With its best horizontal resolution, and most accurate initial conditions, the model runs twice a day, after the conclusion of the data assimilation process. Specifically, the IFS issue time can be set to start at 0 UTC or 12 UTC for the day-ahead predictions, in which the former was used in this analysis. The acquisition procedure comprised several available atmospheric parameters due to their influence over DNI in the operational strategies of a CSP plant. These include GHI, DNI, air temperature, dew point temperature, wind velocity components, total precipitation and total cloud cover. The irradiation parameters given by the model were the surface solar radiation downwards (*ssrd*) and the total sky direct solar radiation (*dsrp*), respectively for GHI and DNI. To compare these predictions with actual observations, the hourly accumulated irradiation values (in J/m^2) from the IFS were divided by 3600 and converted to mean energy flux values (W/m^2). Air and dew point temperatures at 2 m height (*t2m* and *d2m*, respectively, in K) were used to calculate the relative humidity at 2 m height, as described in Eq. (A1) of Section 2 (Appendix A). Other predicted variables were also considered throughout the analysis: the horizontal components of wind velocity (*u* and *v*, in m/s) at 10 m height; the total accumulated precipitation (*tp*, in m), i.e. the sum of convective and large scale precipitation, being accumulated since the beginning of the forecast; surface pressure (*sp*, in Pa), which will be used only in the context of a CSP plant simulation; and the total cloud cover (*tcc*), i.e. the percentage of the sky hidden by all visible clouds.

2.3. Power plant model

The SAM software, version 2017.9.5 (NREL), enables the simulation of several types of CSP systems, in which local atmospheric variables that influence energy production values of a CSP plant are used as input parameters. These not only include DNI but also air temperature, relative humidity, wind speed and surface pressure.

Within the power plant model, a transient system (TRNSYS) is implemented to perform hourly simulations of performance output parameters, providing at the end of each run an annual performance metrics summary. The TRNSYS assembles three components: the first is given by a user-friendly interface, which allows the user to define in detail the setup for the selected CSP plant, including design and control procedures, as well as the input of measured or predicted parameters; the second is the calculation engine, which implements the hourly discretization procedures for the simulation; and the third is a programming interface, which allows the user to define the functions used within the SAM code to obtained performance outputs. A more detail description of the software is available online [36].

For this work, like in a previous study [37], the SAM was used to simulate a conventional linear focus parabolic-trough system installed at EVO location with similar configurations to the 50 MW_e Andasol 3 CSP plant, currently operational in Granada (Spain). The objective in using the Andasol 3 configuration for the simulations of

a CSP plant is not to compare the obtained results in EVO with the ones from the actual power plant installation. Instead, energy outputs based on different Andasol 3 simulations with EVO data are assessed considering measurements, predictions, and improved predictions as input parameters. Particular attention is given to production values outputs, namely to values of electricity generation, represented by the parameter electricity injection to the grid E_G (MW_eh). This parameter is important for the energy management of a power plant since information regarding the power plant's production values for the next hours will help to improve operational decisions performed by the plant's operator. Moreover, the use of improved predictions in these simulations will allow to reduce bad predictions of production values, which can be related to underestimation and overestimation of DNI. Although the inherent overestimation of DNI by the IFS is expected to be present in the estimated values of E_G (when compared with measured-based E_G values), previous results [37] have shown the potential that forecasted data has in the daily operational strategy of a CSP plant. It is also important to consider the subsequent strategies that result from the available E_G estimates from the simulations. In this context, generic operational strategies are also proposed accordingly, as discussed in the Section 5.

3. Methodology

3.1. Evaluation metrics

Due to forecasting inaccuracies in NWP, hourly predictions of DNI have a characteristic bias when compared with local measurements. Overestimation is expected under an overcast sky due to the known underestimation of the radiative effects of clouds. In global models, such as the IFS, this effect is augmented during partly cloudy days. Under very clean atmospheres, DNI predictions have the tendency to underestimate measurements due to the use of monthly mean aerosol values instead of actual values.

In order to quantify the forecast error and compare the performance of different forecasts, it is important to compute the forecasting accuracy. Although several conventional metrics exist, to determine the most appropriate ones depends on the user [38]. For instance, CSP plant operators can be sanctioned per kWh deviation from the expected production [39]. In such cases, error metrics, which allow operators to perform an accurate estimation of the costs related to forecasting errors, are crucial. Particularly, a very important evaluation metric recommended for the application of electrical grid management is the root mean square error (RMSE), due to the importance that large errors have for the safety of an electrical grid system [40]. Considering the mean square error (MSE) of both forecast and persistence (i.e. persistence of the previous measured 24-h values) models with respect to measurements (MSE_{for} and MSE_{per}, respectively), forecasting ability can be carried out using the MSE based skill score (SS). The SS allows to evaluate the global performance of the forecast model towards measurements, as described by Ref. [41] (Eq. (A2) in Section 2 of Appendix A). Other conventional metrics used to assess the forecast error are the mean bias error (MBE), mean absolute error (MAE), Pearson correlation coefficient (r) and coefficient of determination (R^2). More detailed information concerning the use of these and other error metrics for solar forecasting is available in Ref. [38].

3.2. Applied methods

Several methods have been used in this work to perform a comparative analysis between IFS predictions and local measurements at EVO station. In order to quantify the error metrics obtained, hourly and daily clearness indices of DNI (k_b and K_b, respectively) were considered. These dimensionless parameters are a fundamental tool in solar radiation analysis [12], allowing to define the type of irradiance that reaches the Earth's surface, and to further assess the forecasts towards measurements, e.g. Ref. [42]. Based on DNI, a clearness index close to zero is characteristic of overcast conditions, while a value close to 0.8 frequently occurs under clear sky conditions.

In the present analysis, measured, IFS predicted, and improved IFS predicted data were compared. The statistical results from the corresponding k_b and K_b were considered, similarly to Ref. [28], including the forecasting quality obtained for each method. Besides conventional metrics, probabilistic results from probability density functions (PDF's) were considered, allowing to determine the probability distribution (given by the frequency of occurrence) of k_b and K_b. Moreover, skewness and kurtosis analysis were also used, where the former measures the lack of symmetry in respect to the normal distribution and the latter relates with the presence of outliers in a distribution. Statistical models can also be used to correct the IFS predictions. For instance, regression models, in which a dependent variable, i.e. the predictand, is studied (in this case, measured DNI) considering a set of independent variables, i.e. the predictors (in this case, forecasted data), that influence and have impact over the predictand. Each regression coefficient obtained represents the effect that a predictor has in the predictand over time (at the same time that all other predictors remain constant). These basic regression models can be refined using complex multivariate and non-linear relationships between several predictors and the predictand, providing better estimations. In this work, three regression models are used to correct hourly predicted DNI. The first model consists in a simple regression model (SRM), based on a third-degree polynomial fit. The fitting method is based on the use of regression coefficients obtained between measured DNI (i.e. the predictand) and the predicted DNI (i.e. the predictor) from the first year as input to adjust the second year of predicted DNI. The second model is a linear multivariate regression model (MRM1), which uses an interactive *stepwise function* with an adjusted r-squared criterion. This function performs all possible combinations between predictors to find the best fitting option, in this case a second-degree polynomial is considered. The atmospheric predictors used in the MRM1 are: GHI^{IFS}, DNI^{IFS}, GHI^{TOA}, DNI^{TOA}, air temperature ($Temp^{IFS}$), relative humidity (Rh^{IFS}), wind velocity (W^{IFS}), total precipitation ($Prec^{IFS}$) and total cloud cover (Tcc^{IFS}). Then, by including the previous hour (i-1) of measured DNI and GHI as predictors to the MRM1 setup, a compound multivariate regression model (MRM2) is created to perform next-hour (i) predictions of DNI accordingly to the following relation:

$$DNI_i^{\mathrm{MRM2}} = F\left(\begin{array}{c} GHI_{i-1}^{OBS}, DNI_{i-1}^{OBS}, GHI_i^{IFS}, DNI_i^{IFS}, GHI_i^{TOA}, DNI_i^{TOA}, \\ Temp_i^{IFS}, Rh_i^{IFS} W_i^{IFS}, Prec_i^{IFS}, Tcc_i^{IFS} \end{array}\right) \quad (1)$$

where function F is adjusted so that the DNI prediction (DNI_i^{MRM2}) of the first year is closer to the predictand (DNI_i^{OBS}) for the same year, including the previous hour of measured GHI and DNI (GHI_{i-1}^{OBS} and DNI_{i-1}^{OBS}, respectively) as predictors. The function F is then applied to the second year of data for validation of the forecast improvement. Regarding the use of previous hour from measured data, only DNI and GHI were considered in the MRM2, since using other available measured variables would require a higher computational cost, with not significant improvement in the forecast. That is, increasing the number of predictors would lead to more complex polynomials, where the adjustments obtained would not improve significantly the hourly DNI, as compared with

the use of measured irradiances.

It should be noted that several polynomial terms, and respective metrics, were obtained after applying linear multivariate regression for hourly and daily adjustments of MRM1 (Table A1 and Table A2, respectively) and MRM2 (Table A3 and Table A4, respectively) using the *stepwise function*. More detail information regarding these can be seen in the Appendix A (section 3), including all possible iterations between predictors and predictand. After running the *stepwise function*, for the hourly adjustments of MRM1, nine predictors were considered, while for the daily adjustments, only five predictors were used. In the case of MRM2 adjustments, in which two more predictors were added (i.e. DNI_{i-1}^{OBS} and GHI_{i-1}^{OBS}) to the previous MRM1 setup, hourly adjustments considered ten predictors, while for the daily adjustments five predictors were used.

4. Results

4.1. IFS predictions

A first analysis was carried out between measured and predicted DNI over two consecutive years, i.e. from July 1st 2017 to June 30th 2018 and from July 1st 2018 to June 30th 2019. The respective statistical and descriptive results are presented and summarized in Table 1, showing how the IFS predictions behave in comparison with the EVO measured data. During these periods, the annual predicted DNI obtained was remarkably close to the observed one, with very slight overestimation (first year) and underestimation (second year) of the measured values. For instance, mean annual values of ≈480.38 and ≈ 502.04 W/m^2 predicted by the IFS corresponded to an overestimation of ≈0.09 W/m^2 and an underestimation of ≈0.01 W/m^2 for the first and second year, respectively. Moreover, these small differences were respectively attended with a MBE of ≈ -0.05 and ≈ 0.01 W/m^2. The overall good performed of the IFS is also shown by the annual availability obtained values, which were close to the expected regional ones (i.e. above 2100 kWh/m^2/year). This is clearly seen by very small relative differences obtained between annual measured and predicted availabilities (ΔE_b), particularly in the second year, where a value of ≈0.002% was found. Regarding the obtained annual standard deviation (STD), a smaller deviation was registered for the IFS in the second year (≈288.77 W/m^2), i.e. ≈8.01 W/m^2 less than the measured one. Despite the close approximation between the annual values, the RMSE found between hourly values shows the high variability that exists between hourly predicted and measured DNI, mainly due to cloud and aerosol misrepresentation. Nevertheless, such values are found to be consistent with the ones obtained in solar radiation forecasting, e.g. Ref. [40,41], reinforcing the need to improve DNI predictions, as this work aim at. A smaller RMSE of ≈186.20 W/m^2 was obtained in the second year, in comparison to the error associated with measurements. For the hourly r, values of ≈0.85 and ≈ 0.84 were found in the first and second year, respectively, corresponding to an R^2 of ≈0.72 and ≈ 0.71. Considering the daily correlations, values in the order of ≈0.91 and ≈ 0.83 were found respectively for r and R^2 in both years. Such high correlations on the daily scale are expected to be found, since the daily summations filter the hourly variability, in which cloud and aerosol misrepresentations are most noticed.

From the first to the second year of data, an overall decrease in the deviations was observed. This may be related to different intra-annual atmospheric variability. In fact, both measured and predicted data showed less variability in the second year. This can also be associated to the occurrence of less clouds, which resulted in a higher annual availability (2200 kWh/m^2/year), i.e. ≈95 W/m^2 more than in the first year.

In the context of assessing the error associated to the IFS original predictions towards local measurements of DNI, hourly clearness indices (k_b) and respective PDF's were also calculated for each year, as shown in Fig. 1. As expected, close to null-values of k_b, a cluster of values was obtained, as a consequence of the prediction overestimation (due to the misrepresentation of clouds) towards measurements during overcast periods. For instance, during a cloudy period, measurements yield k_b values close to zero while the IFS predictions consider values up to 0.6. As opposed to this, close to high values of k_b, another cluster of hourly values was found, corresponding to clear sky conditions (particularly, very clean atmospheric days), in which an underestimation of the predictions towards measurements occurs. This underestimation is most likely to result from a sub-estimation of the radiative effects towards subgrid clouds and, most importantly, to the use of an aerosol climatology, which overestimates the effect of the aerosols under such conditions. For instance, close to k_b values above 0.7, e.g. during a sunny day that occurs after a rainy day, the actual aerosol concentration in the atmosphere is very low, as opposed to the climatologic aerosol value implemented in the model. During very clean atmosphere conditions, the relation between predicted and measured data was depicted by a smaller dispersion of k_b values in comparison with the ones obtained under overcast and partly cloudy conditions. Particularly, between both extremities, i.e. during partly cloudy periods, there was a high distribution of hourly values that resulted from clouds passing over the measuring equipment, in which the forecast model had difficulties in representing these at the hourly scale. A similar behaviour was observed in both years, as previously discussed. Moreover, the PDF's allowed to observe the frequency of occurrence of k_b values, in which both of the previous discussed clusters (i.e. for low and high values of k_b) were clearly identified. A summary of the statistical results between IFS and measured based k_b values during the second year is presented in Table 2. During this preliminary analysis, an hourly SS of ≈0.66 was found for the second year, being similar to the value obtained for the previous year (not shown here).

When considering daily values, a general improvement of the deviation between predicted and measured values of K_b was found for both years, as shown in Fig. 2. The results, based on the daily availabilities of DNI, showed that the previous overestimation of

Table 1
Statistical and descriptive analysis summary between measured and IFS predicted DNI over two consecutive years in Évora (southern Portugal), from July 1st 2017 to June 30th 2018 and from July 1st 2018 to June 30th 2019. Several annual statistical and error metrics are presented. These include: standard deviation (STD); root mean square error (RMSE); mean absolute error (MAE); mean bias error (MBE); Skewness and Kurtosis; annual DNI availability (E_b) and respective relative differences (ΔE_b); hourly and daily correlation coefficients (r_{hourly}, r_{daily}); hourly and daily coefficient of determination (R^2_{hourly}, R^2_{daily}). Results are presented considering only the daylight period.

	Year 1		Year 2	
	Measurements	IFS	Measurements	IFS
Mean (W/m^2)	480.29	480.38	502.05	502.04
Median (W/m^2)	528.33	506.80	557.52	552.47
STD (W/m^2)	353.42	296.78	347.05	288.77
RMSE (W/m^2)	187.80		186.20	
MAE (W/m^2)	135.38		135.94	
MBE (W/m^2)	−0.05		0.01	
Skewness	−0.113	−0.198	−0.180	−0.311
Kurtosis	1.459	1.597	1.527	1.690
E_b (kWh/m^2/year)	2105	2105	2200	2199
ΔE_b (%)	0.019		0.002	
r_{hourly}	0.847		0.844	
R^2_{hourly}	0.718		0.712	
r_{daily}	0.910		0.912	
R^2_{daily}	0.829		0.832	

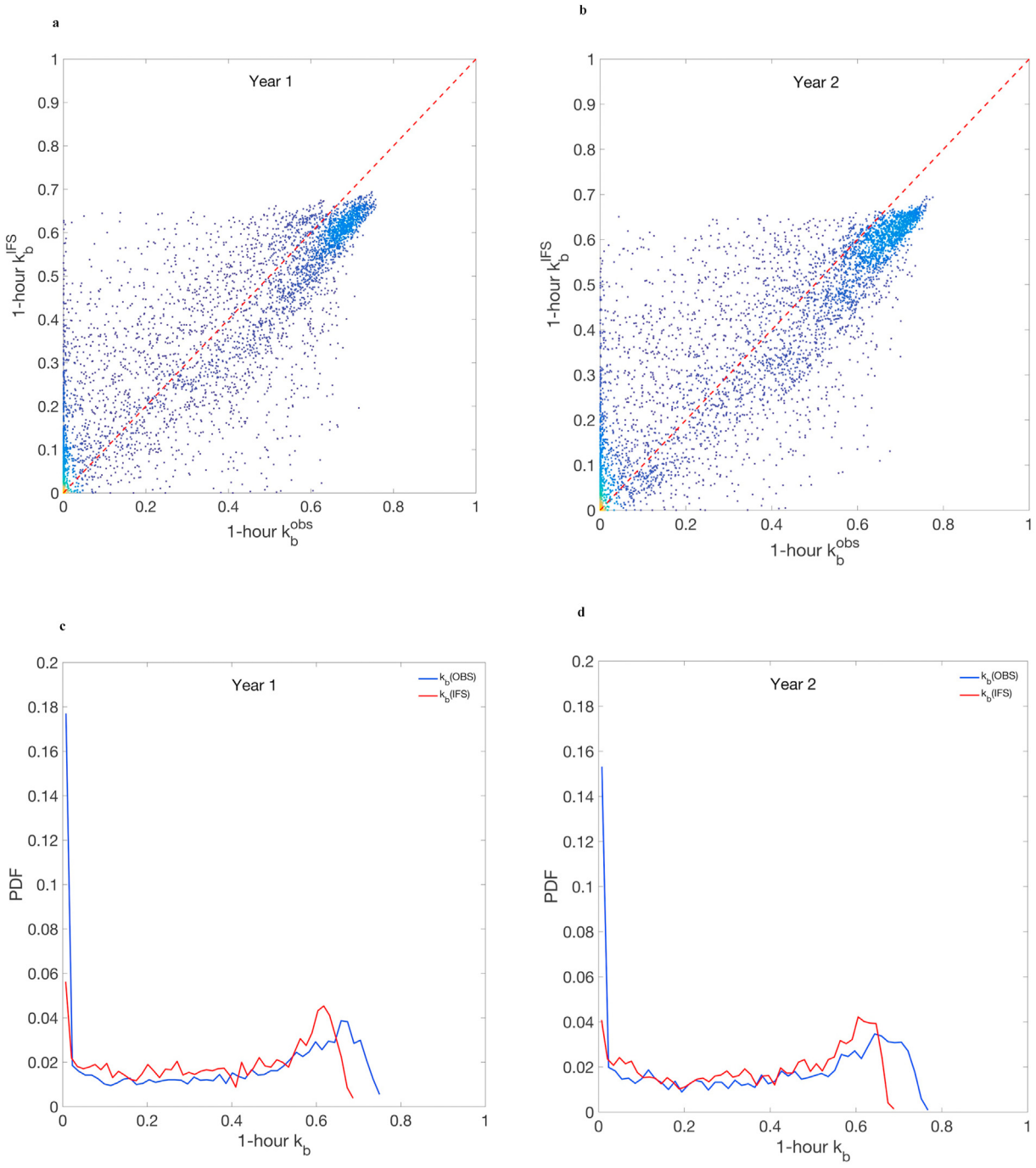

Fig. 1. Hourly (a, b) clearness indices for DNI (k_b) between measurements (OBS) and predictions (IFS) considering two consecutive years of data in Évora, from July 1st 2017 to June 30th 2018 (year 1) and from July 1st 2018 to June 30th 2019 (year 2), with the identity line $y=x$ being also represented (red-dashed line). The respective hourly probability density functions (PDF's) are also shown (c, d). (For interpretation of the references to colour in this figure legend, the reader is referred to the Web version of this article.)

the model close to null K_b values was significantly reduced, leading to higher correlations and lower errors. As previously discussed, at this scale, such effect is expected in NWP, since that the IFS, like most NWP models, has difficulties in predicting the precise location and moment when a variation of DNI occurs, particularly from 1 h to the next. For instance, cloud formation, advection and dissipation, result from complex microphysics process that can occur at sub-grid and sub-hourly scales, and therefore the model will not be able to represent them precisely. When considering daily values of DNI, temporal phase errors are filtered, allowing the IFS to provide satisfactory results when compared with local daily measured based values. This was showed by the narrowing of K_b values towards the identity line in Fig. 2, which depicted a closer behaviour between predicted and measured daily data, although the underestimation of the model during clear sky conditions still prevailed. The respective daily PDF's, besides showing a reduction of the error in comparison with the hourly results, showed a high inter-daily variability, corresponding to the different atmospheric conditions from one day to the other. Such effect is important, especially for the proposed adjusted models at the daily scale. The statistical

Table 2
Statistical summary of hourly clearness indices for DNI (k_b) between measurements and predictions (IFS, SRM, MRM1 and MRM2) for a one year (July 1st 2018 to June 30th 2019) in Évora (southern Portugal). Correlation coefficient (r), coefficient of determination (R^2), root mean square error (RMSE), mean bias error (MBE), mean absolute error (MAE) and skill score (SS) are presented. The SS is calculated towards a referenced persistence model (i.e. measurements time series displaced 24 h ahead).

	Year 2			
	IFS	SRM	MRM1	MRM2
R	0.846	0.849	0.866	0.929
R^2	0.716	0.720	0.750	0.864
RMSE	0.137	0.136	0.129	0.095
MAE	0.100	0.099	0.092	0.062
MBE	1.855×10^{-4}	5.091×10^{-4}	0.003	7.834×10^{-4}
SS	0.656	0.661	0.697	0.835

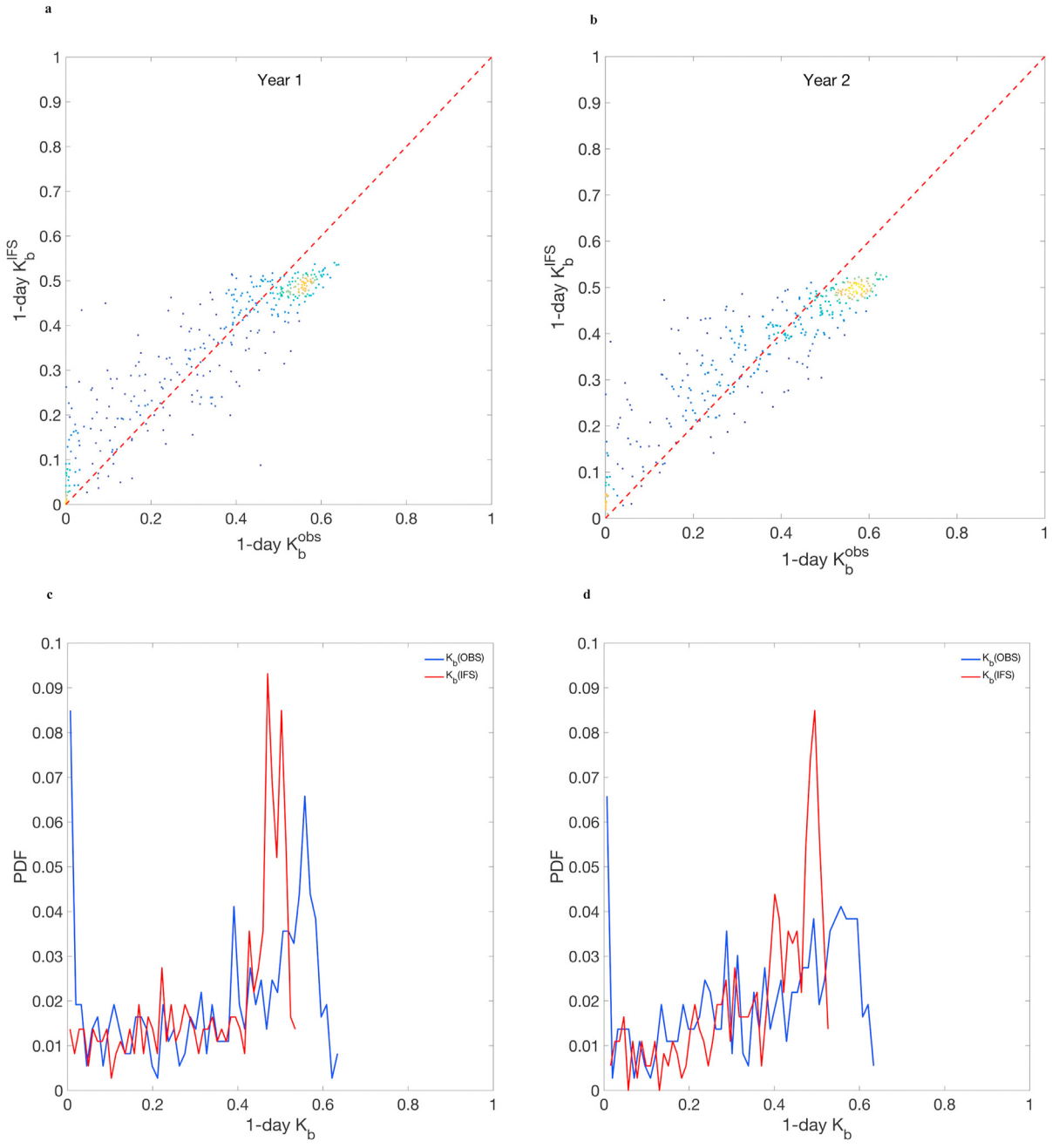

Fig. 2. Daily (a, b) clearness indices for DNI (K_b) between measurements (OBS) and predictions (IFS) for two consecutive years in Évora, from July 1st 2017 to June 30th 2018 (year 1) and from July 1st 2018 to June 30th 2019 (year 2), with the identity line $y=x$ being also represented (red-dashed line). Respective daily probability density functions (PDF's) are also shown (c, d). Daily values were calculated through DNI availabilities (kWh/m^2), i.e. the sum of each 24-h period. (For interpretation of the references to colour in this figure legend, the reader is referred to the Web version of this article.)

Table 3
Statistical summary of daily clearness indices for DNI (K_b) between measurements and predictions (IFS, SRM, MRM1 and MRM2, for one year of data in Évora (southern Portugal), from July 1st 2018 to June 30th 2019. Correlation coefficient (r), coefficient of determination (R^2), root mean square error (RMSE), mean bias error (MBE), mean absolute error (MAE) and skill score (SS) are presented. The SS is calculated towards a referenced persistence model (i.e. measurements time series displaced 24 h ahead).

	Year 2			
	IFS	SRM	MRM1	MRM2
R	0.892	0.897	0.911	0.899
R^2	0.795	0.804	0.831	0.809
RMSE	0.090	0.084	0.077	0.082
MAE	0.071	0.063	0.056	0.058
MBE	−0.002	−0.002	0.006	0.005
SS	0.734	0.772	0.805	0.779

results obtained are summarized in Table 3, where a daily SS of ≈0.73 was attained between measurements and predictions for the second year. The daily values, which consider predicted daily availabilities, also allowed to visualize the potential of the IFS regarding the definition of operational strategies of a CSP plant. Such information is particularly important to a plant operator concerning the expected DNI availability and the distribution of energy dispatchability for the next day.

To further improve hourly predictions of DNI, post-processing methods can be applied. Since the ecRad (cycle 43R3) was implemented in July 2017, this work only considers the period of two years. This can be seen as a limitation regarding statistical downscaling methods (e.g. the application of perfect prognosis) for the correction of DNI, particularly towards daily adjustments. However, MOS techniques are suitable for the present analysis, in which the previous results allowed to set up a statistical reference henceforth, using the first year to improve hourly predictions in the second year.

4.2. Spatial average

Prior to the application of regression analysis, a simple error correction was performed by implementing a spatial average that considers the closest grid points to the actual measuring location, instead of using the nearest global model grid point. The method has some benefits [43], in which small improvements can be attained when considering hourly predictions of DNI from the IFS. This was the case when performing an average from a 3 x 3 grid points (corresponding to an area of about 18 km × 18 km), centred in the nearest grid point to the EVO geographic coordinates. The spatial average, which was separately applied for both years, yield very similar results. Overall, when compared with the nearest point to the measuring location, results from the second year showed an hourly correlation increase of ≈0.51% and a decrease of ≈1.20% in the RMSE.

It should be noted that an increase in the number of available grid points used for averaging could be an option, however the resulting average DNI would be unrepresentative of the exact location of study. Moreover, performing the spatial average considering daily values did not provide any improvement, since intra-day variability is already reduced by the daily summation. For this matter, to further improve hourly DNI predictions, different techniques should be pursued to significantly reduce the associated error.

4.3. Simple regression model (SRM)

Regression coefficients obtained from a polynomial adjustment in first year, between measured and predicted values of DNI, can be used to correct the IFS predictions in the second year. To this end, several polynomials were tested, in which a third-degree polynomial was found to provide the best results with the IFS for the application of the SRM.

Results showed small improvements and the presence of a non-linear relation, as shown by the k_b obtained values (Fig. 3a). Comparing these results with the ones previously obtained between the IFS original predictions and measurements (Table 2), an increase of ≈0.35% and a decrease of ≈0.73% were found for the r and RMSE, respectively. An hourly SS of ≈0.66 was attained using the SRM, corresponding to an increase of ≈0.76%. When comparing the respective PDF's (Fig. 3b), the improvement is clear, particularly for higher values of k_b (i.e. in the absence of clouds) where hourly SRM values are closer to the observed behaviour than the ones obtained with the IFS (Fig. 1c).

A similar procedure but for the daily availabilities (Fig. 4a) revealed correlations of ≈0.90 and a SS of ≈0.77 (Table 3), i.e. an increase of ≈0.56% and ≈5.05% in comparison with the IFS daily K_b's, respectively.

These results, besides showing improvements using simple regression methods, evidence the need of using more complex approaches that can lead to a more substantial reduction of the error associated to hourly predicted DNI. One example is to include other variables related to DNI modulation for the polynomial adjustment, as discussed in the following sections.

4.4. Multivariate regression model (MRM1)

As it was shown in the previous section, adjusting only DNI forecast to the DNI observations, does not improve substantially the forecasts. This is a result of the complex nature of the DNI related physical processes. Thus, in this subsection, other forecasted meteorological variables along with predicted DNI are considered to match the observed DNI, using a multivariate regression technique. This technique uses the observed DNI as the objective function and determines the optimal combination of coefficients and input variables (in this case, the forecasted variables) to approximate the predictions to the observations. The method has the advantage of simulating some of the physical phenomena that actual occur, allowing to consider interaction terms between variables (e.g. predicted DNI with predicted temperature).

In this context, like in the previous section, regression coefficients, which resulted from the adjustment made between predictions and measurements for the first year, were used to correct the IFS predictions in the second year with the inclusion of eight new predictors. These include the same hour predicted variables, i.e. GHI, irradiances calculated at TOA (GHI^{TOA}, DNI^{TOA}), air temperature, relative humidity, wind velocity, total precipitation and total cloud cover. Due to the large number of predictors, the resulting model MRM1 was found to best perform through a second-degree polynomial fitting with the *stepwise function*. It

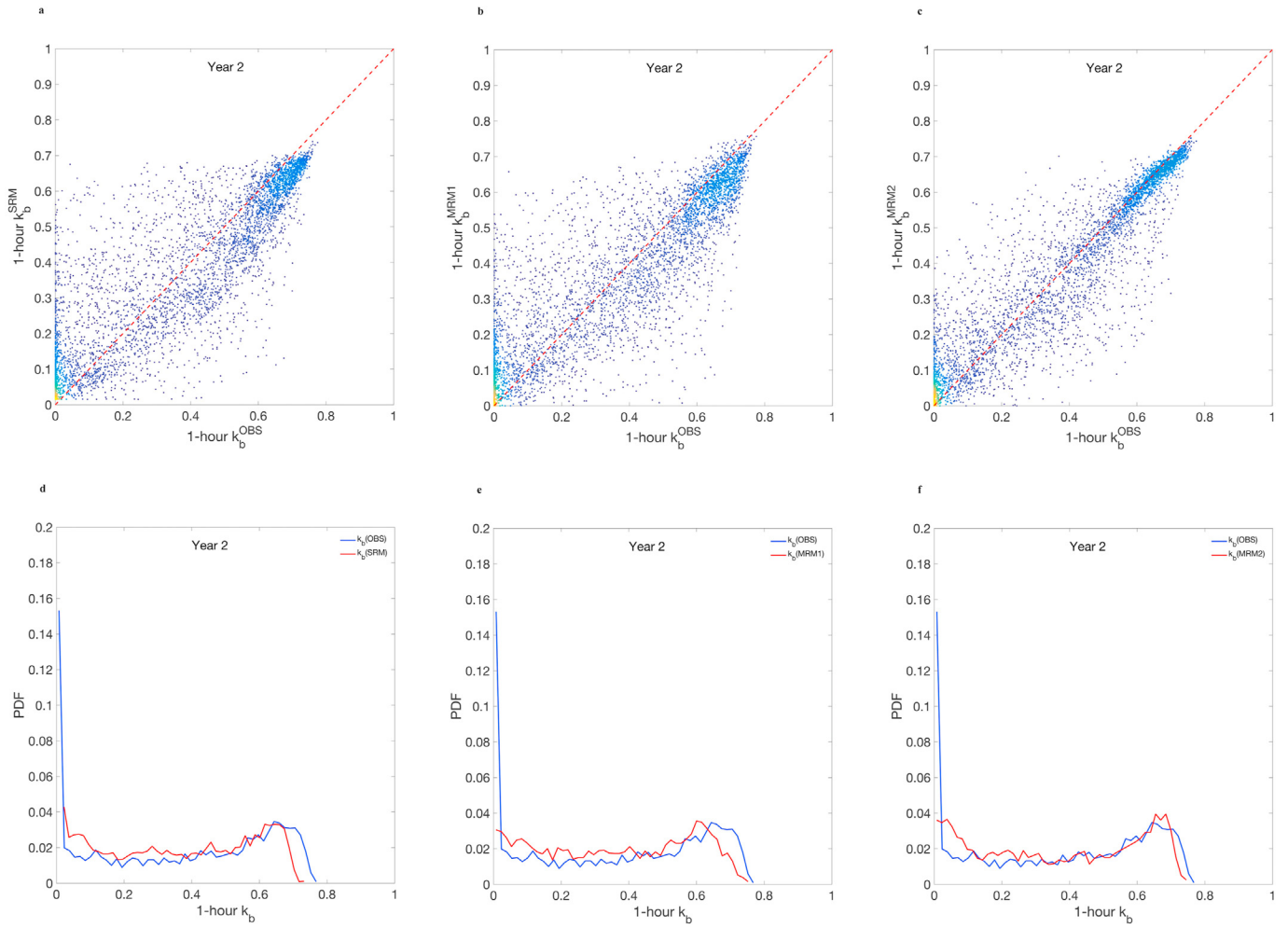

Fig. 3. Hourly clearness indices for DNI (k_b) between measurements (OBS) and improved DNI predictions with (a) SRM, (b) MRM1 and (c) MRM2, where the identity line $y=x$ is represented as a red-dashed line. Analysis is performed over one year of data in Évora (southern Portugal), from July 1st 2018 to June 30th 2019. The respective hourly probability density functions (PDF's) are also depicted (d, e and f). (For interpretation of the references to colour in this figure legend, the reader is referred to the Web version of this article.)

should be noted that when running the *stepwise function*, negative values can result from the multivariate correction of the original IFS data; especially for low observed and predicted DNI values. With this method, a total of 121 negative values were found to occur. In such cases, the original IFS predicted values of the second year of data were maintained. The application of the *stepwise function* for MRM1 was based on the best fitting found through an iterative process that tested 43 different formulations between predictand and all predictors (Table A1, Appendix A).

When performing an analogous method of multivariate regression but to daily DNI availabilities, daily mean values of air temperature, relative humidity, wind velocity, precipitation and cloud cover, were considered. In the case of solar radiation variables, availability values (i.e. the sum of each 24-h periods) were used. The resulting daily adjustment considered 11 different formulations between daily predictand and predictors (Table A2, Appendix A). After performing the correction to the originally predicted availabilities, 7 negative values were found, being the corresponding IFS daily predictions maintained instead.

Results showed that the hourly k_b values obtained, presented in Fig. 3b, and **3e**, illustrate further improvements attained through the MRM1, in comparison to simple linear regression methods. Particularly, during cloudy conditions, i.e. close to null-values of k_b, there is a reduction in the previous overestimation of the predictions towards measurements. It is also observed that for clear sky conditions, there is also a compensation in the underestimation of the predictions. From its original value (i.e. from the IFS) to the value obtained with MRM1, an increase of ≈2.36% in the correlation was attained, together with an overall decrease in the errors, such as ≈5.84% in the RMSE (Table 2). Regarding the hourly SS, a value of ≈0.70 was found, corresponding to an increase of ≈6.25% from the original value. Daily values (Fig. 4b and 4e), which resulted from the polynomial adjustment expressed in Table A2 (Appendix A), showed K_b values with correlations of ≈0.91 and RMSE of ≈0.08 (Table 3). Moreover, an increase of ≈9.55% in the daily SS was obtained in relation to the original value found when using the IFS daily predictions.

In the next section, a new addition to MRM1 is carried out by including the previous hour of measured GHI and DNI as predictors in the case of the hourly analysis. While for the daily analysis, the previous day of measured availability is used to improve the IFS day-ahead predictions.

4.5. Compound multivariate regression model (MRM2)

As means to optimize the MRM1 outputs, the proposed MRM2 was created using the same setup as MRM1, but with the inclusion of the previous hour measured GHI and DNI to the former MRM1

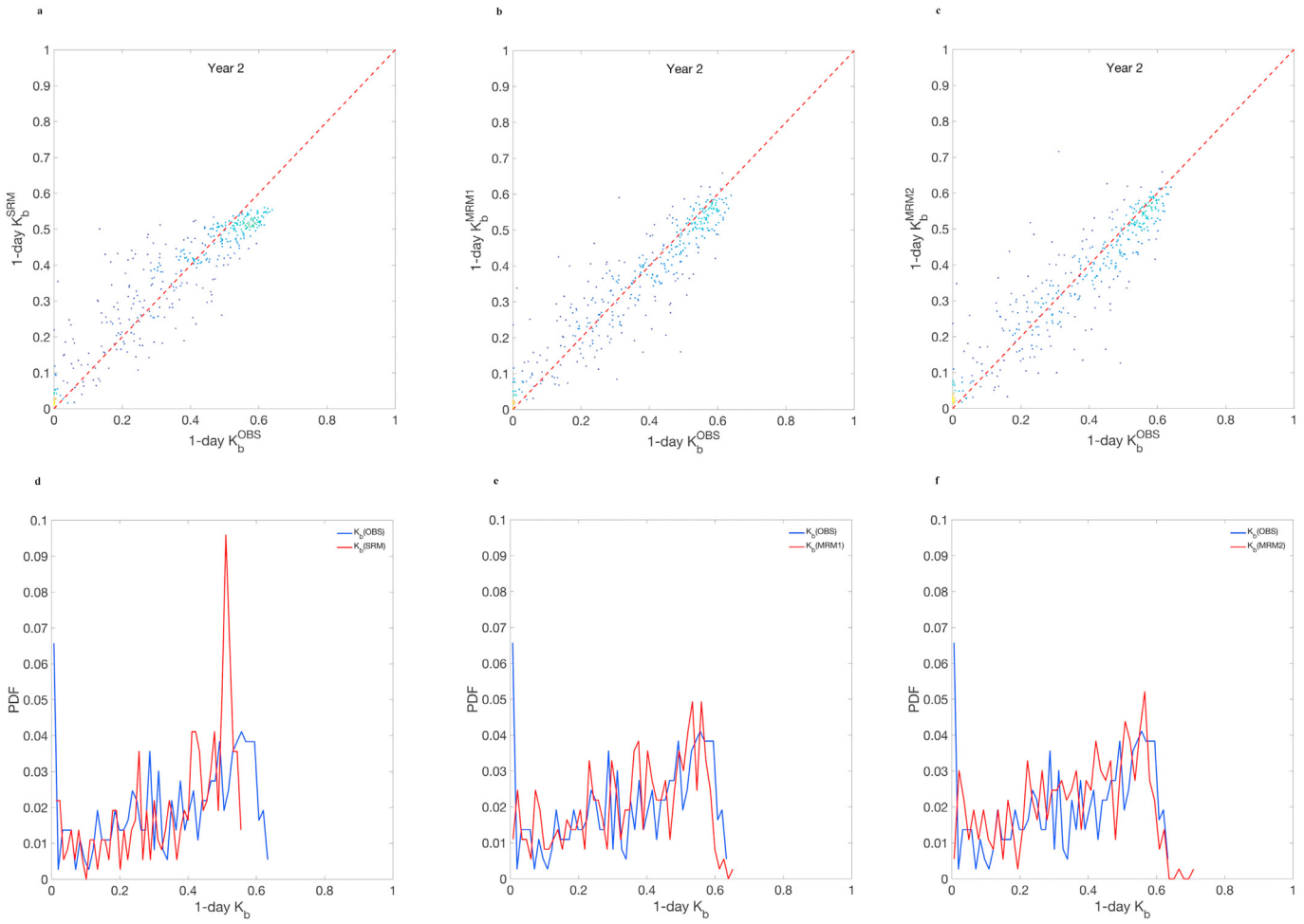

Fig. 4. Daily clearness indices for DNI (K_b) between measurements (OBS) and improved DNI predictions with (a) simple regression model (SRM), (b) multivariate regression model (MRM1) and (c) compound multivariate regression model (MRM2), with identity line $y=x$ represented as a red-dashed line. Analysis is performed over one year of data in Évora (southern Portugal), from July 1st 2018 to June 30th 2019. The respective hourly probability density functions (PDF's) are also being depicted (d, e and f). Daily values are calculated through DNI availabilities (kWh/m^2), i.e. the sum of each 24-h period. (For interpretation of the references to colour in this figure legend, the reader is referred to the Web version of this article.)

predictors. The resulting iterative process tested 50 different formulations between predictand and all predictors (i.e. a total of 11 predictors), as shown in Table A3 (Appendix A). As before with the MRM1, negative values (a total of 84) were obtained for the MRM2 during the regression procedure. Likewise, these values were maintained by the original IFS predicted values, as well as for the first forecast of the day (right after sunrise).

When compared with the IFS hourly values, the MRM2 significantly improves DNI predictions, as shown by the obtained k_b values (Fig. 3c and **d**). The results depict a narrowing towards the identity line $y=x$, i.e. closer to a linear relation than the previous results obtained. In addition to a lower occurrence of overestimated k_b values close to zero, a smaller dispersion of values was also attained for partly cloudy conditions, as well as less underestimated k_b values during clear sky conditions. As shown in the statistical summary (Table 2), an hourly correlation of $\approx$0.93 and a SS of $\approx$0.84 were found, corresponding to increases of $\approx$9.81 and $\approx$ 27.29%, together with a general decrease of the errors.

For the daily availability analysis, the IFS predicted availability of the first day was preserved. Moreover, daily DNI availabilities (Table 3), in which the previous day availability value was used to forecast the next day, resulted from the polynomial adjustment presented in Table A4 (Appendix A). After 23 different formulations, the best fitting found produced 8 negative values, in which the IFS forecasted values were maintained. The K_b values found with this method are showed in Fig. 4c, and **4f**, where high correlations and low errors between adjusted predictions and measurements were found. A daily correlation of $\approx$0.90 and an SS of $\approx$0.78 were obtained for the second year of data. In comparison with the original predicted value obtained with the IFS, these correspond to increases of $\approx$0.78 and $\approx$ 6.13%, respectively.

Despite a dependency on measurements taken in the previous hour or previous day (depending on the case of study), the MRM2 method presents itself as the best fitting found when using multivariate analysis. Through the use of the previous hour of measured DNI and GHI, the model allowed to achieve the best results with significant improvements for the hourly values in comparison with the other presented methods. Moreover, it is possible to observe that for daily availabilities, the improvements obtained are not as significant as the ones obtained on the hourly basis. This is due, in part, to the fact that the IFS daily predictions are already satisfactory, making it more difficult to achieve further

improvements. Another important reason is the fact that only one year of data is being used to correct DNI. This affects particularly the daily correction, in which the daily data can be nearly twelve times less than the data used for the hourly correction. For this matter, in the context of MRM2 daily predictions, more statistical information is required than the one used for this analysis. Thus, with more data (i.e. with an increased number of years) to perform the MRM2 daily adjustments, better predictions with less dispersion of values towards the measured ones from one day to the next should occur.

4.6. Application to CSP operation

After applying different methodologies to improved IFS forecasts, the following two-steps methodology is proposed for their implementation as a tool in CSP operations: i) the use of daily MRM1 improved DNI availabilities to define the generic operation strategy for each day, as suggested by the authors in Ref. [37]; and ii) the application of the improved hourly MRM2 improved DNI predictions to refine hour-by-hour the operation strategy throughout each day, similarly to nowcasting techniques [47]. In summary, using this information for the optimization of CSP plants is fundamental, since precise day-ahead forecasts of DNI allow to predict the day-ahead CSP plant's electricity generation. In addition to improved daily strategies based on different estimates of DNI availability, these can then be further refined with the use of hourly corrections, particularly from MRM2. Focus to these subjects will be given in the next section.

5. CSP operations with improved forecasts

5.1. Power plant daily strategies

Considering the previous results, improved forecasts can now be used for better operational strategies regarding CSP plant's energy management. Such strategies can be implemented on the hourly basis, to optimize energy use throughout the day (being related to short periods of solar intermittency), and, particularly, on the daily basis. This allows the plant operator to decide on how and when to sell the predicted electrical energy generated by the plant at a premium tariff in the electrical market. Information concerning the potential that day-ahead forecasts of DNI have in the operation of CSP systems is available in literature, see Ref. [37,44,45], where recommended strategies for typical days (i.e. days with different weather conditions) are proposed.

This section focuses the use of contingency tables with daily measured and predicted (IFS, SRM, MRM1 and MRM2) availabilities separated by different ranges, according to the previously defined strategies. Such tables aim to evidence the improved accuracy of daily availability range predictions with the use of the correction methods discussed previously. An improved prediction implies a better day-ahead planning regarding a plant operation strategy. This has the potential to lead, if properly articulated with the improved hourly predictions, to an overall enhancement of the solar to electricity conversion procedure. This will be reflected in an increase of the plant's efficiency (e.g. by enabling higher temperatures of the superheated steam in the power block), as well as its dispatchability (e.g. by smoothing temperature variations at the solar field outlet of the heat transfer fluid). The improved hourly predictions will be based on the MRM2 model, which was shown to be the best correction method. Thus, this analysis has the objective of combining improved daily availability predictions with improved hourly forecasts of DNI to increase a power plant operation reliability. Using such combined strategy would certainly improve the electrical energy production and its value, reducing the final levelized cost of electricity, i.e. the ratio between the sum of the discounted total cost during the lifetime of a plant and the sum of the discounted total amount of electrical energy delivered. Consequently, the client's electricity bill would also be reduced, (another strong reason to optimize CSP plants). Although such life cycle analysis is out of scope of the present analysis, it can certainly be carried out in future studies.

Results for the daily availabilities from the IFS, SRM, MRM1 and MRM2, respectively in Tables A5, A6, A7 and A8 (Appendix A), were obtained for a period of one year (from July 1st 2018 to June 30th 2019). In these tables, the number of occurrences when predictions coincide with measurements correspond to the 'Hits' (marked in green), whereas the corresponding success rate (%) was calculated considering the total number of measured availabilities values. The range by which this evaluation was carried out is divided in four intervals, which go from overcast to clear sky conditions, corresponding to different strategies defined for the corresponding atmospheric conditions that have distinct effects over a CSP plant electrical production [37]. As expected, all day-ahead correction models provide satisfactory results, with prediction accuracies generally above 50%, mainly due to the reduction of the intra-day variability, as a consequence of the daily summation. This includes the original IFS day-ahead predictions, which depict the highest daily success rates of 'Hits' between 3 and 9 kWh/m^2/day ($\approx$68.48 and 88.14%, respectively). The daily adjustments were able to significantly increase the day-ahead estimations accuracy during overcast and very clean atmospheric conditions. Success rates of 'Hits' between $\approx$70.89 and 73.42% were respectively found for the MRM2 and for both SRM and MRM1, corresponding to cloudy days (from 0 to 3 kWh/m^2/day). Considering clear sky days (from 9 to 13 kWh/m^2/day), success rates of $\approx$75 and 77.63% were respectively found for the MRM1 and for both SRM and MRM2. Overall, when planning CSP daily operational strategies, a plant operator can rely on the correction models, particularly the MRM2 if longer time-series are available, which can be complemented with the IFS daily predictions during partly cloudy periods. Then, during the day, the hour-ahead strategy could be improved by the hourly predicted DNI value based on the MRM2 (as discussed in the next section).

5.2. Power plant simulation

With the available data, i.e. measurements, IFS forecasts and corrected forecasts, during a one year period, hourly values of DNI and meteorological variables were used as input parameters for the simulation of a CSP plant with similar configurations to the Andasol 3 using the SAM. The corresponding electricity injected into the grid values (E_G, MW_eh), generated by each simulation, based on measured and predicted values (IFS, SRM, MRM1 and MRM2), were

Table 4
Hourly electrical energy injected into the grid (E_G, MW_eh) results through the SAM simulations based on measurements (OBS) and predictions (IFS, SRM, MRM1 and MRM2). One year of data was considered in each run for Évora (southern Portugal). The SAM simulations were performed with similar configurations to the Andasol 3 CSP plant. Correlation coefficient (r), coefficient of determination (R^2), root mean square error (RMSE), mean absolute error (MAE), mean bias error (MBE), total E_G, and relative differences (ΔE_G, %), are presented.

	OBS	IFS	SRM	MRM1	MRM2
R	–	0.89	0.89	0.90	0.97
R^2	–	0.79	0.79	0.82	0.93
RMSE (MW_eh)	–	11.38	11.25	10.40	6.29
MAE (MW_eh)	–	4.11	4.08	3.61	1.85
MBE (MW_eh)	–	−0.82	−0.62	−0.33	−0.11
E_G (MW_eh/year)	166,914	174,086	172,339	169,795	167,880
ΔE_G (%)	–	4.30	3.25	1.73	0.58

then compared and discussed accordingly. To perform this simulation in the SAM, input variables that influence the plant's annual performance (i.e. DNI, air temperature, relative humidity, surface pressure and wind velocity) are considered in each run based on measured or predicted data. Moreover, it is important to have in consideration that the results obtained assume all the plant's power consumption losses, including periods of non-production (i.e. nights and overcast periods) and a constant derating value of 4%.

The Andasol 3 annual performance results (Table 4) showed annual energies of ≈166,914 MW_eh/year for the measured data, while for the IFS predictions a value of ≈174,086 MW_eh/year was obtained. The predicted annual overestimation is a result of the IFS tendency to overestimate measured values during overcast periods, in which the plant efficiency is higher due to lower temperatures. Such conditions occur more frequently than very clean atmospheric periods, in which the IFS has the tendency to underestimate measured values (i.e. when the plant's efficiency is lower). Using the IFS improved DNI predictions, and the meteorological predicted data, an annual value of ≈172,339 MW_eh/year was found for the SRM, while for the MRM1 ≈169,795 MW_eh/year was reached. However, it is with the MRM2 that the best results based on hourly E_G values were attained, with ≈167,880 MW_eh/year and a relative difference of ≈0.58%, being the closest value to the one based on measurements. Moreover, a rough estimation of the economic value of the improved MRM2 predictions can also be performed, considering the average selling price of electricity of 7c€/kW_eh [46] for large industrial customers in Europe. In this context, considering the simulation that run the DNI observations for the considered year, the profit of the plant would be ≈ 11.68 M€, while the one expected with IFS original forecasted data would be higher, i.e. ≈12.19 M€, corresponding to a difference (Δ_{IFS}) of ≈0.51 M€. On the other hand, if the MRM2 predictions are used instead, such value would be ≈ 11.75 M€, i.e. an Δ_{MRM2} of ≈0.07 M€ would be attained. This allows to calculate the difference between the two predicted values obtained ($\delta = \Delta_{IFS} - \Delta_{MRM2}$), which can in some way quantify the increased profit with the use of the proposed improved predictions. Such value would be around 0.44 M€ (i.e. ≈3.80% of the total profit). A full range of possible economic improvements can only be accessed with a thorough CSP simulation that allows the implementation of hourly and daily operational strategies, which is out of the scope of this analysis. However, such implementations should be carried out in future studies.

6. Conclusions and future perspectives

In order to improve hourly and daily predictions of DNI from the ECMWF global model, statistical post-processing methods were applied to the provided 24-h forecasts of the IFS. Considering two consecutive years of predicted and measured data in Évora, the attained corrected predictions resulted from the use of simple techniques, suitable to be used from the operational point of view, including linear and multivariate regression analysis. It was observed that best results were achieved with the use of the MRM2 correction model. Through the use of hourly clearness indices, the MRM2 showed a high correlation (≈0.93), representing an increase of ≈9.81% in comparison with the IFS original value. Moreover, the MRM2 demonstrated a skill score (SS) of ≈0.84, i.e. ≈27.29% higher than the one obtained with the IFS. As expected, on the daily scale, the proposed correction models showed satisfactory results due to the reduction of the cloud overestimation characteristic of the hourly predictions, as a consequence to the daily summation. Lower daily errors and higher correlations were found using the daily correction models, where a daily SS of ≈0.78 was found for the MRM2. However, to further improve the MRM2 daily predictions, more than one year of data is required due to the high inter-daily variability of DNI. Nevertheless, daily contingency tables were created to provide generic strategies to a plant operator under different atmospheric conditions. On a daily basis, predictions can be used with the corrected values, particularly for overcast and clear sky days, while during partly cloudy periods the original daily availabilities from the IFS are maintained. Operational strategies based on day-ahead predictions can also be refined throughout the day using the MRM2, which was shown to be the most suitable model to be used on the hourly time scale. The application of measured and predicted data in the simulation of a conventional linear parabolic-trough power plant (similar to the Andasol 3 CSP) allowed to compare the electrical energy injected into the grid (E_G). The results showed that E_G hourly values were best predicted with the MRM2. Additionally, a preliminary economic analysis of the simulated plant showed that the MRM2 predicted hourly values of E_G allowed to enhance the plant's profit in ≈0.44 M€, as compared to the use of the original IFS forecasts.

To further improve this analysis, future studies should focus on the use of more robust post-processing techniques. At the same time, these should be of easy application to the plant operator in order to facilitate operational procedures, which sometimes can require fast decisions. Future corrections should give more emphasis in correcting hourly values during overcast and partly cloudy periods, i.e. periods of high energy demand, in which hourly overestimations towards measured values still remain one of the main challenge's in solar forecasting. For instance, the inclusion of other important parameters in the MRM2, such as the previous hour of measured aerosol optical depth values. Another method that can be beneficial for improvement of short-terms forecasts of DNI forecasts, is the integration of an all sky imager based nowcasting system, such as the one installed nearby Évora [47]. Since the SAM uses a single strategy, i.e. to produce electricity whenever there is DNI available, more emphasis should be given to a model that makes use of daily operational strategies [54], including the use of hourly values of the MRM2, as it was shown to be the best correction model found in this work.

CRediT authorship contribution statement

Francis M. Lopes: Conceptualization, Investigation, Resources, Methodology, Supervision, The concept of this work, investigation, resources, and the implemented methodology, were made by, ECMWF forecasts were obtained by, System Advisor Model simulations were carried out by, All authors have reviewed the article prior to the resubmission, ECMWF forecasts were obtained by, All authors have reviewed the article prior to the resubmission, Supervision, All authors have reviewed the article prior to the resubmission. have supervised this work. **Ricardo Conceição:** Writing - review & editing, Data curation, Funding acquisition, Data curation, Formal analysis, and post-processing analysis, writing and editing procedures, were done by. **Hugo G. Silva:** Writing - review & editing, Data curation, Funding acquisition, Data curation, Formal analysis, and post-processing analysis, writing and editing procedures, were done by. **Rui Salgado:** Supervision, All authors have reviewed the article prior to the resubmission. have supervised this work. **Manuel Collares-Pereira:** Supervision, All authors have reviewed the article prior to the resubmission. have supervised this work.

Declaration of competing interest

The authors declare that they have no known competing financial interests or personal relationships that could have appeared to influence the work reported in this paper.

Table A1
Hourly multivariate regression metrics obtained through the use of the stepwise function considering a second-degree polynomial adjustment of DNI (MRM1) during one year (from July 1st 2018 to June 30th 2019).

	MRM1			
Terms	Estimates	SE	tStat	pValue
'(Intercept)'	-3.59×10^{4}	1.27×10^{4}	−2.83	4.65×10^{-3}
'x_1'	8.18	2.10	3.90	9.84×10^{-5}
'x_2'	1.30	3.20	0.41	0.68
'x_3'	−3.56	1.40	−2.54	0.01
'x_4'	47.51	17.80	2.67	7.64×10^{-3}
'x_5'	174.09	65.97	2.64	8.35×10^{-3}
'x_6'	29.45	17.65	1.67	0.10
'x_7'	327.68	130.22	2.52	0.01
'x_8'	-1.35×10^{4}	4.18×10^{3}	−3.22	1.29×10^{-3}
'x_9'	3.54×10^{3}	850.58	4.16	3.25×10^{-5}
'$x_1 \bullet x_3$'	-8.65×10^{-4}	1.90×10^{-4}	−4.55	5.56×10^{-6}
'$x_1 \bullet x_4$'	-5.04×10^{-3}	1.45×10^{-3}	−3.48	5.07×10^{-4}
'$x_1 \bullet x_5$'	−0.03	7.20×10^{-3}	−3.90	9.68×10^{-5}
'$x_1 \bullet x_6$'	-4.43×10^{-3}	2.33×10^{-3}	−1.90	0.06
'$x_1 \bullet x_8$'	−16.42	10.71	−1.53	0.13
'$x_1 \bullet x_9$'	−0.06	0.11	−0.50	0.62
'$x_2 \bullet x_4$'	-1.88×10^{-3}	2.24×10^{-3}	−0.84	0.40
'$x_2 \bullet x_5$'	0.02	6.65×10^{-3}	2.26	0.02
'$x_2 \bullet x_6$'	2.70×10^{-3}	3.50×10^{-3}	0.77	0.44
'$x_2 \bullet x_7$'	−0.01	9.54×10^{-3}	−1.39	0.16
'$x_2 \bullet x_8$'	−5.94	18.78	−0.32	0.75
'$x_2 \bullet x_9$'	0.99	0.21	4.78	1.83×10^{-6}
'$x_3 \bullet x_4$'	3.57×10^{-3}	1.02×10^{-3}	3.52	4.44×10^{-4}
'$x_3 \bullet x_6$'	-4.27×10^{-3}	1.64×10^{-3}	−2.60	9.42×10^{-3}
'$x_3 \bullet x_8$'	15.35	7.20	2.13	0.03
'$x_3 \bullet x_9$'	−0.84	0.16	−5.13	3.02×10^{-7}
'$x_4 \bullet x_5$'	−0.11	0.04	−2.49	0.01
'$x_4 \bullet x_6$'	−0.02	0.01	−1.40	0.16
'$x_4 \bullet x_7$'	−0.22	0.09	−2.52	0.01
'$x_4 \bullet x_9$'	−2.50	0.59	−4.24	2.33×10^{-5}
'$x_5 \bullet x_6$'	−0.15	0.08	−1.97	0.05
'$x_5 \bullet x_7$'	−0.85	0.47	−1.80	0.07
'$x_5 \bullet x_9$'	−6.39	3.07	−2.08	0.04
'$x_6 \bullet x_7$'	0.20	0.15	1.39	0.16
'$x_6 \bullet x_9$'	−2.81	1.00	−2.80	5.06×10^{-3}
'$x_7 \bullet x_9$'	−23.55	5.83	−4.04	5.49×10^{-5}
'x_1^2'	7.81×10^{-4}	1.42×10^{-4}	5.51	3.83×10^{-8}
'x_2^2'	4.24×10^{-4}	1.49×10^{-4}	2.85	4.44×10^{-3}
'x_3^2'	-1.69×10^{-4}	5.91×10^{-5}	−2.85	4.35×10^{-3}
'x_4^2'	−0.02	6.30×10^{-3}	−2.51	0.01
'x_5^2'	−0.35	0.15	−2.38	0.02
'x_6^2'	−0.04	0.02	−2.52	0.01
'x_8^2'	4.68×10^{5}	1.20×10^{5}	2.34	0.02
'x_9^2'	246.04	52.12	4.72	2.42×10^{-6}

Table A2
Daily multivariate regression metrics obtained through the use of the stepwise function considering a second-degree polynomial adjustment of DNI (MRM1) during one year (from July 1st 2018 to June 30th 2019).

	MRM1			
Terms	Estimates	SE	tStat	pValue
'(Intercept)'	−5.98	4.06	−1.47	0.14
'x_1'	1.27	0.50	2.53	0.01
'x_2'	0.40	0.22	1.78	0.08
'x_5'	0.05	0.08	0.69	0.49
'x_6'	0.21	0.09	2.41	0.02
'x_9'	3.88	1.53	2.53	0.01
'$x_1 \bullet x_6$'	−0.02	6.16×10^{-3}	−2.97	3.16×10^{-3}
'$x_2 \bullet x_5$'	−0.01	0.01	−1.13	0.26
'$x_6 \bullet x_9$'	−0.11	0.03	−3.63	3.29×10^{-4}
'x_1^2'	0.05	0.02	2.46	0.01
'x_5^2'	-2.21×10^{-3}	2.88×10^{-3}	−0.77	0.44
'x_6^2'	-9.48×10^{-4}	4.81×10^{-4}	−1.97	0.05

Table A3
Hourly multivariate regression metrics obtained through the use of the stepwise function considering a second-degree polynomial adjustment of DNI that uses the previous measured irradiance (MRM2) values during one year (from July 1st 2018 to June 30th 2019).

	MRM2			
Terms	Estimates	SE	tStat	pValue
'(Intercept)'	-2.18×10^{4}	7.11×10^{3}	−3.06	2.21×10^{-3}
'x_1'	7.48	1.74	4.30	1.74×10^{-5}
'x_2'	−4.45	2.12	−2.10	0.04
'x_3'	0.39	0.18	2.21	0.03
'x_4'	33.55	10.60	3.16	1.57×10^{-3}
'x_5'	−10.92	2.74	−3.98	6.96×10^{-5}
'x_6'	−18.20	9.64	−1.89	0.06
'x_7'	103.16	72.98	1.41	0.16
'x_9'	−257.21	647.21	−0.40	0.69
'x_{10}'	−2.82	1.00	−2.81	4.96×10^{-3}
'x_{11}'	0.46	1.77	0.26	0.80
'$x_1 \bullet x_2$'	1.20×10^{-3}	3.48×10^{-4}	3.46	5.53×10^{-4}
'$x_1 \bullet x_3$'	-1.02×10^{-3}	2.56×10^{-4}	−3.97	7.25×10^{-5}
'$x_1 \bullet x_4$'	-4.25×10^{-3}	1.24×10^{-3}	−3.43	6.07×10^{-4}
'$x_1 \bullet x_5$'	−0.03	5.73×10^{-3}	−6.04	1.70×10^{-9}
'$x_1 \bullet x_6$'	-3.49×10^{-3}	1.81×10^{-3}	−1.93	0.05
'$x_1 \bullet x_9$'	−0.43	0.11	−3.95	7.90×10^{-5}
'$x_1 \bullet x_{10}$'	7.82×10^{-4}	1.58×10^{-4}	4.96	7.44×10^{-7}
'$x_1 \bullet x_{11}$'	-7.67×10^{-4}	3.00×10^{-4}	−2.55	0.01
'$x_2 \bullet x3'$	-5.72×10^{-4}	2.38×10^{-4}	−2.41	0.02
'$x_2 \bullet x_4$'	2.84×10^{-3}	1.47×10^{-3}	1.94	0.05
'$x_2 \bullet x_5$'	0.02	9.13×10^{-3}	2.53	0.01
'$x_2 \bullet x_6$'	1.26×10^{-3}	2.49×10^{-3}	0.50	0.61
'$x_2 \bullet x_9$'	0.66	0.22	2.98	2.93×10^{-3}
'$x_2 \bullet x_{10}$'	-1.57×10^{-3}	2.99×10^{-4}	−5.27	1.47×10^{-7}
'$x_2 \bullet x_{11}$'	1.34×10^{-3}	4.32×10^{-4}	3.10	1.96×10^{-3}
'$x_3 \bullet x_5$'	5.03×10^{-3}	4.73×10^{-3}	1.06	0.29
'$x_3 \bullet x_9$'	−0.30	0.15	−1.99	0.05
'$x_3 \bullet x_{10}$'	8.13×10^{-4}	1.70×10^{-4}	4.78	1.85×10^{-6}
'$x_3 \bullet x_{11}$'	5.20×10^{-4}	2.24×10^{-4}	2.33	0.02
'$x_4 \bullet x_6$'	0.01	6.87×10^{-3}	1.80	0.07
'$x_4 \bullet x_7$'	−0.07	0.05	−1.26	0.21
'$x_4 \bullet x_9$'	0.15	0.48	0.31	0.75
'$x_4 \bullet x_{10}$'	1.70×10^{-3}	6.91×10^{-4}	2.45	0.01
'$x_4 \bullet x_{11}$'	-3.11×10^{-4}	1.23×10^{-3}	−0.25	0.80
'$x_5 \bullet x_6$'	0.04	0.03	1.51	0.13
'$x_5 \bullet x_9$'	2.97	1.79	1.66	0.10
'$x_5 \bullet x_{10}$'	0.03	3.88×10^{-3}	7.06	1.96×10^{-12}
'$x_5 \bullet x_{11}$'	−0.01	6.50×10^{-3}	−1.97	0.05
'$x_6 \bullet x_{10}$'	4.06×10^{-3}	1.34×10^{-3}	3.03	2.44×10^{-3}
'$x_6 \bullet x_{11}$'	-1.97×10^{-3}	2.24×10^{-3}	−0.88	0.38
'$x_7 \bullet x_{10}$'	-6.48×10^{-3}	4.54×10^{-3}	−1.43	0.15
'$x_9 \bullet x_{10}$'	0.35	0.06	5.71	1.24×10^{-8}
'$x_9 \bullet x_{11}$'	−0.27	0.11	−2.40	0.02
'$x_{10} \bullet x_1$'	2.31×10^{-4}	1.30×10^{-4}	1.78	0.08
'x_1^2'	-2.48×10^{-4}	1.82×10^{-4}	−1.37	0.17
'x_3^2'	-1.37×10^{-4}	9.07×10^{-5}	−1.51	0.13
'x_4^2'	−0.01	3.97×10^{-3}	−3.23	1.27×10^{-3}
'x_7^2'	−0.64	0.61	−1.04	0.30
'x_9^2'	50.03	42.74	1.17	0.24
'x_{11}^2'	-6.98×10^{-4}	1.62×10^{-4}	−4.31	1.67×10^{-5}

Table A4
Daily multivariate regression metrics obtained through the use of the stepwise function considering a second-degree polynomial adjustment of DNI that uses the previous measured irradiance values (MRM2) during one year (from July 1st 2018 to June 30th 2019).

MRM2				
Terms	Estimates	SE	tStat	pValue
'(Intercept)'	−2.79	5.97	−0.47	0.64
'x_1'	0.61	1.13	0.54	0.59
'x_2'	−0.81	0.56	−1.44	0.15
'x_5'	0.31	0.15	2.07	0.04
'x_6'	0.25	0.09	2.68	7.81×10^{-3}
'x_9'	−4.84	5.57	−0.87	0.39
'x_{10}'	−0.47	0.18	−2.66	8.09×10^{-3}
'x_{11}'	1.18	0.75	1.59	0.11
'$x_1 \bullet x_2$'	0.08	0.05	1.50	0.13
'$x_1 \bullet x_5$'	−0.07	0.03	−2.62	9.24×10^{-3}
'$x_1 \bullet x_6$'	−0.03	8.80×10^{-3}	−3.14	1.82×10^{-3}
'$x_1 \bullet x_9$'	2.03	0.60	3.37	8.30×10^{-4}
'$x_1 \bullet x_{11}$'	−0.08	0.05	−1.77	0.08
'$x_2 \bullet x_5$'	0.07	0.03	2.06	0.04
'$x_5 \bullet x_9$'	−0.22	0.12	−1.83	0.07
'$x_5 \bullet x_{10}$'	0.04	9.72×10^{-3}	3.88	1.25×10^{-4}
'$x_5 \bullet x_{11}$'	−0.07	0.03	−2.48	0.01
'$x_6 \bullet x_9$'	−0.17	0.05	−3.46	6.06×10^{-4}
'$x_6 \bullet x_{11}$'	6.51×10^{-3}	5.43×10^{-3}	1.20	0.23
'$x_9 \bullet x_{11}$'	−0.74	0.31	−2.38	0.02
'x_1^2'	0.14	0.07	2.07	0.04
'x_5^2'	-3.53×10^{-3}	2.99×10^{-3}	−1.18	0.24
'x_6^2'	-9.45×10^{-4}	4.93×10^{-4}	−1.9	0.06
'x_9^2'	7.39	2.07	3.56	4.17×10^{-04}

Table A5
Contingency table for availability values of DNI (kWh/m^2/day) between observations (OBS) and IFS predictions. A range divided in four intervals defines different weather conditions during a one year period (from July 1st 2018 to June 30th 2019) in Évora (southern Portugal). The total number of measurements (Total OBS) is also presented.

IFS						
OBS		0–3	3–6	6–9	9–13	Total OBS
	0–3	47 (59.49%)	28 (35.44%)	4 (5.06%)	0	79
	3–6	2 (2.17%)	63 (68.48%)	27 (29.35%)	0	92
	6–9	0	12 (10.17%)	104 (88.14%)	2 (1.70%)	118
	9–13	0	1 (1.32%)	37 (48.68%)	38 (50.00%)	76

Table A6
Contingency table for availability values of DNI (kWh/m^2/day) between observations (OBS) and SRM predictions. A range divided in four intervals defines different weather conditions during a one year period (from July 1st 2018 to June 30th 2019) in Évora (southern Portugal). The total number of measurements (Total OBS) is also presented.

SRM						
OBS		0–3	3–6	6–9	9–13	Total OBS
	0–3	58 (73.42%)	17 (21.52%)	3 (3.80%)	1 (1.27%)	79
	3–6	10 (10.87%)	55 (59.78%)	26 (28.26%)	1 (1.09%)	92
	6–9	0	16 (13.56%)	97 (82.20%)	5 (4.24%)	118
	9–13	0	1 (1.32%)	16 (21.05%)	59 (77.63%)	76

Table A7
Contingency table for availability values of DNI (kWh/m^2/day) between observations (OBS) and MRM1 predictions. A range divided in four intervals defines different weather conditions during a one year period (from July 1st 2018 to June 30th 2019) in Évora (southern Portugal). The total number of measurements (Total OBS) is also presented.

MRM1						
OBS		0–3	3–6	6–9	9–13	Total OBS
	0–3	58 (73.42%)	19 (24.05%)	2 (2.53%)	0	79
	3–6	14 (15.22%)	57 (61.96%)	20 (21.74%)	1 (1.09%)	92
	6–9	1 (0.85%)	15 (12.71%)	98 (83.05%)	4 (3.39%)	118
	9–13	0	1 (1.32%)	18 (23.68%)	57 (75.00%)	76

Table A8
Contingency table for availability values of DNI (kWh/m^2/day) between observations (OBS) and MRM2 predictions. A range divided in four intervals defines different weather conditions during a one year period (from July 1st 2018 to June 30th 2019) in Évora (southern Portugal). The total number of measurements (Total OBS) is also presented.

MRM2						
OBS		0–3	3–6	6–9	9–13	Total OBS
	0–3	56 (70.89%)	21 (26.58%)	2 (2.53%)	0	79
	3–6	15 (16.30%)	62 (67.40%)	14 (15.22%)	1 (1.09%)	92
	6–9	1 (1.85%)	11 (9.32%)	97 (82.20%)	9 (7.63%)	118
	9–13	0	1 (1.32%)	16 (21.05%)	59 (77.63%)	76

Acknowledgements

F.M. Lopes and R. Conceição acknowledge the Portuguese Foundation for Science and Technology (FCT) PhD grant (SFRH/BD/129580/2017) and the National Research Infrastructure in Solar Energy Concentration (INIESC, ALT20-03-0145-FEDER-022113) post-doc research grant (BI_POS-DOC_INIESC_II), respectively. H.G. Silva wishes to acknowledge discussions hold with Dr. Klaus Hennecke from the German Aerospace Center (DLR) on related topics to this work that considerably inspired it. Co-funding was also provided by the European Union through the European Regional Development Fund included in the COMPETE 2020 (Operational Program Competitiveness and Internationalization) through the ICT (UID/GEO/04683/2020, POCI-01-0145-FEDER-007690), DNI-ALENTEJO (ALT20-03-0145-FEDER-000011) and ALOP (ALT20-03-0145-FEDER-000004) projects. The authors are grateful to: the Portuguese meteorological service (IPMA), particularly to Jorge Neto, for providing the necessary meteorological data; the European Centre for Medium-Range Weather Forecasts (ECMWF), for the provided forecasts; T. Fasquelle, whose collaboration in previous works that lead to this paper is highly appreciated; and P. Canhoto and E. Abreu, for the maintenance of solar radiation measurements in Évora.

Appendix A

1. Data quality-control

Although there is no definitive procedure for data processing [48], to perform a correct analysis of surface solar radiation, it is important to apply a *posteriori* proper filters to the measured data. Since the nature of the latter is site-dependent, several factors can affect the measured data, as described in Ref. [49]: geographical coordinates (latitude, longitude), astronomical factors (solar declination, daylight hours), geometric factors (solar azimuth angle), physical factors (scattering and absorption effects due to aerosol content present in the atmosphere), terrain topography, surface albedo, nearby structures (e.g. trees, buildings) and meteorological variables (e.g. clouds, air temperature, wind speed, air relative humidity, precipitation). Particularly, remote locations of difficult man-made access often show large missing periods of recorded data (from a few days to several weeks), whether due to equipment malfunction or to sudden power supply shutdowns, which can last up to several hours.

In this context, considering the study location (i.e. southern region of Portugal) and two years of continuous GHI and DNI measurements, the following filters were applied:

a. Only positive values, i.e. daylight hours, are considered.
b. Linear interpolation is performed for gaps greater than 15% of the total number of hours within each day.
c. BSRN Global Network maximum and minimum physically possible limits [50].
d. Deterministic variables, i.e. solar zenith angle, DNI and GHI at the top-of-the-atmosphere (TOA), respectively DNI^{TOA} and GHI^{TOA}, are calculated on an hourly basis, as described by Eq. 2.77 in Ref. [51], considering the geographical coordinates of EVO station and a total solar irradiance at TOA of 1361 W/m^2 [52].

Condition *a* allows to remove irradiance night values (i.e. negative values) from the analysis. In condition *b*, linear interpolation of GHI and DNI is performed for days that have ≈3.5 h (depending on the available number of daylight hours throughout the year) of missing data. In order to refine the analysis, condition *c* is used taking into consideration the physically possible limits for GHI and DNI (shortwave components), allowing to remove any irradiance value measured at surface that is higher than the respective value calculated at TOA (condition *d*). Such abnormal values can be recorded mainly due to equipment mal function.

The application of the proposed filters to the measured radiation data at EVO station resulted in the following percentage of missing data: ≈0.0011% (≈0.096 h) and ≈0.0015% (≈0.13 h) for the first and second years, respectively. Moreover, regarding the local meteorological parameters, ≈0.0076% (≈0.67 h) was found for the first year of measurements, whereas for the second only very few minutes of missing data occurred. These numbers show how well-maintained is the measuring equipment used. For consistency reasons, the same missing periods found in measurements are set equally in the IFS forecasts.

2. Relative humidity and skill score formulas

As described by Ref. [53], the following relation was used to calculate the relative humidity (Rh) considering both ECMWF predicted dew point and air temperatures (T_{dew} and T_{air}, respectively):

$$Rh = \left[6.11 \times 10^{\left(7.5 \times \frac{T_{dew}}{237.7+T_{dew}}\right)} \Big/ 6.11 \times 10^{\left(7.5 \times \frac{T_{air}}{237.7+T_{air}}\right)} \right] \times 100 \quad \text{(A1)}$$

The forecasting skill considered in the analysis made use of the skill score (SS) in regards to the mean square error obtained between measurements and forecast model (MSE_{for}) and measurements and persistence model (MSE_{per}), as described by Ref. [41]:

$$SS = 1 - MSE_{for} \Big/ MSE_{per} \quad \text{(A2)}$$

where an SS equal to one indicates a perfect forecast, negative values of SS mean that the forecast model performs worse than the persistence model, while a null result shows that the forecast model has no improvement towards the persistence model.

3. Multivariate regression tables

In the following tables (**A1**, **A2**, **A3** and **A4**) are all significant and possible relations between predictors and predictand (Terms), the weight (Estimates) that each relation has in the respective adjustment, the standard error (SE) obtained, the t-statistics (tStat), and the p-value (pValue), for both MRM1 and MRM2 hourly and daily adjustments. The following set of predictors were considered for the hourly adjustments: x_1 (DNI_i^{IFS}), x_2 (GHI_i^{IFS}), x_3 (GHI_i^{TOA}), x_4 (DNI_i^{TOA}), x_5 ($Temp_i^{IFS}$), x_6 (Rh_i^{IFS}), x_7 (W_i^{IFS}), x_8 ($Prec_i^{IFS}$), x_9 (Tcc_i^{IFS}), x_{10} (DNI_{i-1}^{OBS}) and x_{11} (GHI_{i-1}^{OBS}), with DNI_i^{OBS} as the predictand. In the case of the daily adjustments, predictors x_1, x_2, x_5, x_6 and x_9 were considered.

4. Daily contingency tables

For the evaluation of daily availability values regarding the operations of a CSP plant, contingency tables were used considering daily measured and predicted (IFS, SRM, MRM1 and MRM2) data for one year in EVO.

References

[1] P. Blanc, B. Espinar, N. Geuder, C. Gueymard, R. Meyer, R. Pitz-Paal, et al., Direct normal irradiance related definitions and applications: the circumsolar issue, Sol. Energy 110 (2014) 561–577, https://doi.org/10.1016/j.solener.2014.10.001.
[2] M. Schroedter-Homscheidt, O. Oumbe, A. Benedetti, J.-J. Morcrette, Aerosols for Concentrating Solar Electricity Production Forecasts: Requirement Quantification and ECMWF/MACC Aerosol Forecast Assessment, American Meteorological Society BAMS, 2013, pp. 903–914, https://doi.org/10.1175/BAMS-D-11-00259.1.
[3] R. Conceição, H.G. Silva, J. Mirão, M. Gostein, L. Fialho, L. Navarte, M. Collares-Pereira, Saharan dust transport to Europe and its impact on photovoltaic performance: a case study of soiling in Portugal, Sol. Energy 160 (2018) 94–102, https://doi.org/10.1016/j.solener.2017.11.059.
[4] R. Conceição, M. Melgão, H.G. Silva, K. Nicoll, R.G. Harrison, A.H. Reis, Transport of the smoke plume from Chiado's fire in Lisbon (Portugal) sensed by atmospheric electric field measurements, Air Qual.Atmosphere.Health 9 (2016) 275–283, https://doi.org/10.1007/s11869-015-0337-4.
[5] A. Callado, P. Escribà, J.A. García-Moya, J. Montero, C. Santos, D. Santos-Muñoz, J. Simarro, Ensemble forecasting, climate change and regional/local responses, in: Dr Pallav Ray (Ed.), In Tech, vol. 1, 2013, https://doi.org/10.5772/55699.
[6] S. Pereira, P. Canhoto, R. Salgado, M.J. Costa, Development of an ANN based corrective algorithm of the operational ECMWF global horizontal irradiation forecasts, Sol. Energy 185 (2019) 387–405, https://doi.org/10.1016/j.solener.2019.04.070.
[7] D. Wilks, Statistical Methods in the Atmospheric Sciences, second ed., vol. 100, 2005, ISBN 9780080456225 (Chapter 6).
[8] M. Rummukainen, Methods for Statistical Downscaling of GCM Simulations, Technical Report (80). ISSN: 0347-2116, Swedish Meteorological and Hydrological Institute, 1997. August 3rd 2020, http://www.smhi.se/polopoly_fs/1.1243221!/RMK_80.pdf. SMHI Reports Meteorology Climatology. Available from:.
[9] W.H. Klein, B.M. Lewis, I. Enger, Objective Prediction of Five-Day Mean Temperatures during Winter, vol. 16, American Meteorological Society, 1959, pp. 672–682, https://doi.org/10.1175/1520-0469(1959)016<0672:OPOFDM>2.0.CO;2.

[10] H.R. Glahn, D.A. Lowry, The use of model output statistics (MOS) in objective weather forecasting, Applied Meteorology 11 (1972) 1203–1211, https://doi.org/10.1175/1520-0450(1972)011<1203:TUOMOS>2.0.CO;2.
[11] W.Y.Y. Cheng, W.J. Steenburgh, Strengths and Weaknesses of MOS, Running-Mean Bias Removal, and Kalman Filter Techniques for Improving Model Forecasts over the Western United States, vol. 22, American Meteorological Society, 2007, pp. 1304–1318, https://doi.org/10.1175/2007WAF2006084.1.
[12] A. Troccoli, J.-J. Morcrette, Skill of direct solar radiation predicted by the ECMWF global atmospheric model over Australia, in: Applied Meteorology and Climatology, American Meteorological Society, 2014, pp. 2571–2587, https://doi.org/10.1175/JAMC-D-14-0074.1.
[13] A. Pérez-Burgos, J. Bilbao, A. de Miguel, R. Román, Analysis of solar direct irradiance in Spain, Energy Procedia (2014) 1070–1076, https://doi.org/10.1016/j.egypro.2014.10.070.
[14] T.N. Krishnamurti, C.M. Kishtawal, T.E. LaRow, D.R. Bachiochi, Z. Zhang, C.E. Williford, S. Gadgil, S. Surendran, Improved weather and seasonal climate forecast from multimodel superensemble, Science 285 (1999) 1548–1550, https://doi.org/10.1126/science.285.5433.1548.
[15] P.L. Houtekamer, H.L. Mitchell, Data Assimilation Using an Ensemble Kalman Filter Technique, vol. 126, American Meteorological Society, 1998, pp. 796–811, https://doi.org/10.1175/1520-0493(1998)126<0796:DAUAEK>2.0.CO;2.
[16] J.W. Lin, J.D. Neelin, Towards stochastic deep convective parameterization in general circulation models, Geophys. Res. Lett. 30 (N4) (2003) 1162, https://doi.org/10.1029/2002GL016203.
[17] J.M. Murphy, D.M.H. Sexton, D.N. Barnett, G.S. Jones, M.J. Webb, M. Collins, D.A. Stainforth, Quantification of modelling uncertainties in a large ensemble of climate change simulations, Nature 430 (7001) (2004) 768–772, https://doi.org/10.1038/nature02771.
[18] J. Berner, G.J. Shutts, M. Leutbecher, T.N. Palmer, A Spectral Stochastic Kinetic Energy Backscatter Scheme and its Impact on Flow-dependent Predictability in the ECMWF Ensemble Prediction System, vol. 66, American Meteorology Society, 2009, pp. 603–625, https://doi.org/10.1175/2008JAS2677.1.
[19] W.I. Hameed, B.A. Sawadi, S.J. Al-Kamil, M.S. Al-Radhi, Y.I.A. Al-Yasir, A.L. Saleh, R.A. Abd-Alhameed, Prediction of solar irradiance based on artificial neural networks, Inventions MDPI 4 (2019) 45, https://doi.org/10.3390/inventions4030045.
[20] G. Reikard, C. Hansen, Forecasting solar irradiance at short horizons: frequency and time domain models, Renew. Energy 135 (2019) 1270–1290, https://doi.org/10.1016/j.renene.2018.08.081.
[21] G. Reikard, S.E. Haupt, T. Jensen, Forecasting ground-level irradiance over short horizons: time series, meteorological, and time-varying parameter models, Renew. Energy 112 (2017) 474–485, https://doi.org/10.1016/j.renene.2017.05.019.
[22] D. Yang, Ensemble model output statistics as a probabilistic site-adaptation tool for satellite-derived and reanalysis solar irradiance, Renew. Sustain. Energy 12 (1) (2020), https://doi.org/10.1063/1.5134731, 016102.
[23] E. Díez, C. Primo, J.A. García-Moya, J.M. Gutiérrez, B. Orfila, Statistical and dynamical downscaling of precipitation over Spain from DEMETER seasonal forecasts, Tellus 57A 3 (2005) 409–423, https://doi.org/10.3402/tellusa.v57i3.14698.
[24] P.G. Kosmopoulos, S. Kazadzis, M. Taylor, E. Athanasopoulou, O. Speyer, P.I. Raptis, et al., Dust impact on surface solar irradiance assessed with model simulations, satellite observations and ground-based measurements, Atmos.-Meas. Tech. 10 (2017) 2435–2453, https://doi.org/10.5194/amt-2017-79.
[25] G. Myhre, D. Shindell, F.-M. Bréon, W. Collins, J. Fuglestvedt, J. Huang, et al., Anthropogenic and natural radiative forcing. Climate Change, in: Midgley (Ed.), The Physical Science Basis. Contribution of Working Group I to the Fifth Assessment Report of the Intergovernmental Panel on Climate Change, Cambridge University Press, 2013, pp. 659–740, https://doi.org/10.1017/CBO9781107415324.018.
[26] S.E. Haupt, P.A. Jiménez, J.A. Jared, B. Kosovic, Principles of meteorology and numerical weather prediction, in: Georges Kariniotakis (Ed.), Renewable Energy Forecasting: from Models to Applications vol. 1, 2017, pp. 3–28, https://doi.org/10.1016/B978-0-08-100504-0.00001-9.
[27] R. Salgado, P.M.A. Miranda, P. Lacarrére, J. Noilhan, Boundary layer development and summer circulation in Southern Portugal, Tethys 12 (2015) 33–34, https://doi.org/10.3369/tethys.2015.12.03.
[28] F.M. Lopes, H.G. Silva, R. Salgado, A. Cavaco, P. Canhoto, M. Collares-Pereira, Short-term forecasts of GHI and DNI for solar energy systems operation: assessment of the ECMWF integrated forecasting system in southern Portugal, Sol. Energy 170 (2018) 14–30, https://doi.org/10.1016/j.solener.2018.05.039.
[29] ISO 9060:1990, Solar Energy – Specification and Classifications of Instruments for Measuring Hemispherical Solar and Direct Solar Radiation, International Organization for Standardization, 2003. Available online from: www.iso.org/standard/16629.html. (Accessed 3 August 2020).
[30] ISO 9059:1990, Solar Energy – Calibration of Field Pyrheliometers by Comparison to a Reference Pyrheliometer, International Organization for Standardization, 2014. Available online from: www.iso.org/standard/16628.html. (Accessed 3 August 2020).
[31] R. Conceição, A.A. Merrouni, D. Lopes, A. Alae, H.G. Silva, E.G. Bennouna, et al., A comparative study of soiling on solar mirrors in Portugal and Morocco: preliminary results for the dry season, AIP Conference Proceedings 2126 (2019) 220001, https://doi.org/10.1063/1.5117760.
[32] T. Haiden, M. Janousek, F. Vitart, L. Ferranti, F. Prates, Evaluation of ECMWF forecasts, including the 2019 resolution upgrade, in: European Centre for Medium-Range Weather Forecasts, Technical Memorandum, vol. 853, 2019, https://doi.org/10.21957/mlvapkke10.21957/vltarm3ql.
[33] R.J. Hogan, A. Bozzo, A flexible and efficient radiation scheme for the ECMWF model, Adv. Model. Earth Syst. 10 (2018) 1990–2008, https://doi.org/10.1029/2018MS001364.
[34] A. Bozzo, S. Remy, A. Benedetti, J. Flemming, P. Bechtold, M.J. Rodwell, J.-J. Morcrette, Implementation of a CAMS-based aerosol climatology in the IFS, in: European Centre for Medium-Range Weather Forecasts, Technical Memorandum, vol. 801, 2017. Available from: https://www.ecmwf.int/sites/default/files/elibrary/2017/17219-implementation-cams-based-aerosol-climatology-ifs.pdf. (Accessed 3 August 2020).
[35] I. Tegen, P. Hollrig, M. Chin, I. Fung, D. Jacob, J. Penner, Contribution of different aerosol species to the global aerosol extinction optical thickness: estimates from model results, Geophysical Research, Atmospheres 102 (23) (1997) 895–915, https://doi.org/10.1029/97JD01864.
[36] N. Blair, A. Dobos, J. Freeman, T. Neises, M. Wagner, T. Ferguson, et al., System Advisor Model, SAM 2014.1.14: General Description, National Renewable Energy Laboratory, Golden, CO, 2014. NREL/TP-6A20-61019.
[37] F.M. Lopes, R. Conceição, H.G. Silva, T. Fasquelle, R. Salgado, P. Canhoto, M. Collares-Pereira, Predicted direct solar radiation (ECMWF) for optimized operational strategies of linear focus parabolic-trough systems, Renew. Energy 151 (2019) 378–391, https://doi.org/10.1016/j.renene.2019.11.020.
[38] C. Coimbra, J. Kleissl, R. Marquez, Overview of solar forecasting methods and a metric for accuracy evaluation, in: Solar Resource Assessment and Forecasting, vol. 8, Elsevier, Waltham, Massachusetts, 2013, ISBN 9780123971777, pp. 183–185.
[39] M. Wittmann, H. Breitkreuz, M. Schroedter-Homscheidt, M. Eck, Case studies on the use of solar irradiance forecast for optimized operation strategies of solar thermal power plants, IEEE.Sel. Top. Appl. Earth.Obs. Remote Sens. 1 (2008) 18–27, https://doi.org/10.1109/jstars.2008.2001152.
[40] M. Schroedter-Homscheidt, A. Benedetti, N. Killius, Verification of ECMWF and ECMWF/MACC's global and direct irradiance forecasts with respect to solar electricity production forecasts, Meteorologische Zeitschrift 26 (2016) 1–19, https://doi.org/10.1127/metz/2016/0676. PrePub Article.
[41] R. Perez, E. Lorenz, S. Pelland, M. Beauharnois, G.V. Knowe, K. Hemker Jr., et al., Comparison of numerical weather prediction solar irradiance forecasts in the US, Canada and Europe, Sol. Energy 94 (2013) 305–326, https://doi.org/10.1016/j.solener.2013.05.005.
[42] T.R. Ayodele, A.S.O. Ogunjuyigbe, Prediction of monthly average global solar radiation based on statistical distribution of clearness index, Energy 90 (2015) 1733–1742, https://doi.org/10.1016/j.energy.2015.06.137.
[43] I.T. Jolliffe, D.B. Stephenson, Forecast Verification: A Practitioner's Guide in Atmospheric Science, 5.4.4, Wiley, New York, 2003, ISBN 9780470660713, pp. 106–110.
[44] F.M. Lopes, R. Conceição, H.G. Silva, R. Salgado, P. Canhoto, M. Collares-Pereira, Predictive value of short-term forecasts of DNI for solar energy systems operation, AIP Conference Proceedings 2126 (2019) 190010, https://doi.org/10.1063/1.5117707.
[45] F.M. Lopes, R. Conceição, H.G. Silva, T. Fasquelle, R. Salgado, P. Canhoto, M. Collares-Pereira, Short-term forecasts of DNI from an integrated forecasting system (ECMWF) for optimized operational strategies of a central receiver system, Energies 12 (2019) 1368, https://doi.org/10.3390/en12071368.
[46] B.F. Towler, The Future of Energy, first ed., vol. 8, Academic Press, 2014, ISBN 9780128010273, pp. 183–184.
[47] N. Bijan, S. Wilbert, N. Blum, P. Kuhn, T. Schmidt, Z. Yasser, et al., Evaluation of an all sky imager based nowcasting system for distinct conditions and five sites, AIP Conference Proceedings (2020) (accepted for publication).
[48] C.A. Gueymard, J.A. Ruiz-Arias, Extensive worldwide validation and climate sensitivity analysis of direct irradiance predictions from 1-min global irradiance, Sol. Energy 128 (2016) 1–30, https://doi.org/10.1016/j.solener.2015.10.010, 2016.
[49] A.J. Gutiérrez-Trashorras, E. Villicaña-Ortiz, E. Álvarez-Álvarez, J.M. González-Caballín, J. Xiberta-Bernat, M.J. Suarez-López, Attenuation processes of solar radiation. Application to the quantification of direct and diffuse solar irradiances on horizontal surfaces in Mexico by means of an overall atmospheric transmittance, Renew. Sustain. Energy Rev. 81 (2018) 93–106, https://doi.org/10.1016/j.rser.2017.07.042.
[50] C.N. Long, E.G. Dutton, BSRN global network recommended QC tests, V2.0, Available online: https://bsrn.awi.de/fileadmin/user_upload/bsrn.awi.de/Publications/BSRN_recommended_QC_tests_V2.pdf. August 3rd 2020, , 2002.
[51] S.A. Kalogirou, Solar Energy Engineering: Processes and Systems, second ed., vol. 2, Elsevier, 2014, ISBN 978-0123972705, pp. 51–63.
[52] S.K. Solanki, N.A. Krivova, J.D. Haigh, Solar irradiance variability and climate, Annu. Rev. Astron. Astrophys. 51 (2013) 311–351, https://doi.org/10.1146/annurev-astro-082812-141007.
[53] M.G. Lawrence, The relationship between relative humidity and the dewpoint temperature in moist air, in: A Simple Conversion and Applications, American Meteorological Society, 2005, https://doi.org/10.1175/BAMS-86-2-225.
[54] T. Fasquelle, Q. Falcoz, P. Neveu, F. Lecat, G. Flamant, A termal model to predict the dynamic performances of parabolic trough lines, Energy 141 (2017) 1187–1203, https://doi.org/10.1016/j.energy.2017.09.063.